NTNU

Norwegian University of
Science and Technology

Process Simulation of a Hybrid Fuel Cell System for Clean and Highly Efficient Offshore Power with Carbon Capture

Ørjan Nymark Melle

Chemical Engineering and Biotechnology
Submission date: April 2017
Supervisor: Magne Hillestad, IKP
Co-supervisor: Ivar Wærnhus, CMR Prototech

Norwegian University of Science and Technology
Department of Chemical Engineering

Ørjan Nymark Melle

Process Simulation of a Hybrid Fuel Cell System for Clean and Highly Efficient Offshore Power with Carbon Capture

Master's Thesis - TKP4900
for the degree of M.Sc. in Chemical Engineer

Trondheim, April 2017

Norwegian University of Science and Technology
Faculty of Natural Science and Technology
Department of Chemical Engineering

NTNU
Innovation and Creativity

NTNU

Norwegian University of Science and Technology

Master's Thesis - TKP4900
for the degree of M.Sc. in Chemical Engineer

Faculty of Natural Science and Technology
Department of Chemical Engineering

Master's Thesis at NTNU,

Printed by NTNU-trykk

Abstract

Today, offshore power is mainly produced onsite by gas turbines and the process is responsible for the majority of the CO_2-emissions from the Norwegian offshore industry. To reduce CO_2-emissions offshore, electrification of the Norwegian continental shelf by long power cables from renewable onshore power production has been on the political agenda since the mid nineties, however, due to cost, only a few facilities are currently supplied by onshore power. By replacing the gas turbines with a highly effective hybrid fuel cell system, CMR Prototech has suggested an alternative solution that combined with carbon capture and storage may potentially produce clean and highly efficient offshore power (CHEOP).

To replace today's offshore gas turbines, a topside concept capable of delivering 32 MW of electrical power is required. In that context, CMR Prototech has developed a proposed P&ID of a scaled-down CHEOP process that delivers 3.2 MW of electrical power at an electrical efficiency of 60% without carbon capture.

In this work, a flow-sheet model of CMR Prototech's suggested CHEOP process with carbon capture was simulated in Aspen HYSYS to investigate its potential to produce clean and highly efficient power offshore. However, to be able to implement the proposed process in HYSYS, the membrane reactor of the CHEOP process was replaced by an already existing process route for syngas production and hydrogen separation as there is no specific unit operations that models the behaviour of membrane reactors in Aspen HYSYS, and to model one is outside the scope of this thesis.

Hence, based on the nominal operating conditions of CMR Prototech's proposed CHEOP process and a literature review of hydrogen production technologies, an equilibrium-based flow-sheet model of the CHEOP process with carbon capture was developed in Aspen HYSYS to investigate its potential performance in this work. Furthermore, a sensitivity analysis and a heat integration were also performed to study how the process behave and its potential for further improvements.

The simulation results show that at nominal operating conditions, the process has a net electrical power output of 2.89 MW and an electrical plant efficiency of 56.4%, which is excellent considered that the carbon capture process is included. Furthermore, approximately 400 kW of high quality excess heat from the oxyfuel-combustor are available for utilization in the reformer that will increase the hydrogen production and thus also the electrical power output and efficiency of the process if utilized. However, even though the additional heat is utilized, the SOFC is responsible for approximately 40% of the electrical power generation of the process. In CMR Prototech's proposed process the SOFC is only responsible for approximately 22% of the total power generation. This means that due to the energy demand of the reformer, a quite big SOFC will be needed in the more conventional process simulated in this work. This may become a problem with regards to size and weight on offshore facilities.

Preface

This Master's thesis was written in the fall/spring of 2016/17. It concludes the 5 year Master's program in Chemical Engineering and Biotechnology at the Norwegian University of Science and Technology, leading to the degree of M.Sc. in Chemical Engineering. My final year at NTNU was spent as a part of the research group in Environmental Engineering and Reactor Technology within the Department of Chemical Engineering. The work performed in this thesis is a result of several meetings with CMR Prototech and Professor Magne Hillestad in the spring of 2016.

I would like to thank my supervisor Professor Magne Hillestad for weekly meetings and interesting challenges during my thesis. I would also like to thank CMR Prototech for giving me the opportunity to work on such an interesting topic and specially thanks to Ivar Wærnhus for great feedback and guidance along the way. I am also grateful for the feedback and help provided by Crina Ilea Silvia, Torstein Bishop, Morten Thomas Emhjellen and Vidar Skjervold, but most of all I am grateful for the support, guidance and encouragement I received from my family and closest friends during this period.

Declaration of Compliance

I hereby declare that this is an independent work according to the exam regulations of the Norwegian University of Science and Technology (NTNU).

Trondheim, April 4, 2017
Ørjan N. Melle

Contents

List of Tables

List of Figures

Chapter 1

Introduction

It is no longer a doubt that human influence has a tremendous effect on the climate system. According to the Intergovernmental Panel of Climate Change's Fifth Assessment Report, many of the observed climate changes, like increasing temperatures, rising sea levels and diminishing amounts of snow and ice, are extremely likely to be a consequence of the increasing amount of anthropogenic greenhouse gas (GHG) emissions since the pre-industrial era (1). Due to the large amounts present in the atmosphere, carbon dioxide (CO_2) is considered to be the largest contributor to the global climate changes. Between 1750 and 2011, about 2000 gigatons of CO_2 have been released to the atmosphere. About half of these anthropogenic emissions have occurred the last 40 years (1). The recent anthropogenic GHG emissions are the highest in history. As a consequence, global warming is becoming a world challenging problem.

From 1990 to 2014, the Norwegian oil and gas sector had a rapid growth due to discoveries of several new oil and gas fields. In the same period, several operating fields have reached the final stages of production, which are more energy consuming. In addition, new technology have also made it possible to operate fields longer and longer. Due to the increased activity, the emissions of the oil and gas sector have increased by approximately 80% in this period, which have made it the main contributor of Norway's GHG emissions since 2007 if transportation are divided into aviation, maritime and road traffic (2). In 2015, 53.9 million tons of CO_2-equivalents were emitted in Norway. The oil and gas sector was responsible for 28.0% of these emission. It is therefore of huge interest to find solutions that can reduce the GHG emissions of the Norwegian oil and gas sector.

Today, the vast majority of offshore power is generated by gas turbines. Natural

gas (NG) is burned in a combustion chamber together with compressed air and produces flue gas, typically consisting of $C, CO, CO_2, H_2O, O_2, N_2, NO_x$ and SO_x depending on the quality of the NG. Then, the resulting flue gas is expanded through a gas turbine that drives a generator and electrical power is produced. The exhaust from the turbines are released into the air. The efficiency of such plants are typically in the range of 30-35% (3, 4).

On some newer and larger facilities with higher energy demands, combined cycle gas turbine (CCGT) plants are used. In such plants, waste heat recovery units (WHRU) are used to recover some of the heat of the hot exhaust gas from the turbines (5). The recovered heat can either be utilized as heat or to produce high pressure steam (HPS). HPS can further be used to produce more electricity in a steam turbine generator. Depending on the access of cooling water, CCGT plants can achieve efficiencies close to 60% (4, 5). Offshore, size and weight are limiting factors, thus single gas turbines are often preferred before CCGT plants. Either way, in both plant designs the exhaust is released directly into the air, and because of that, offshore energy production is the major contributor to GHG emissions form the oil and gas sector (6).

Several measures have been initiated to try to reduce the GHG emissions from the oil and gas sector. Since it was introduced in the offshore industry in 1991, the CO_2 tax has been one of the main initiatives to reduce the emissions of the sector. Together with the emission scheme, which included the offshore industry in 2008, they have been able to create an awareness of the needs for a more energy efficient power production offshore (6). Several cost effective measures like process optimization, operational improvements and coordination of power production between platforms (e.g. Snorre, Gullfaks, Oseberg and Ekofisk) have been implemented, but as technological improvements have led to more fields in operation, both in terms of new and old fields with extended production periods, such measures have proven to be inadequate as the emissions continue to increase.

Another initiative that may have the potential to reduce the emissions of the oil and gas sector is electrification of the continental shelf. Electrification implies to replace the offshore power produced by onsite gas turbines with preferably renewable power produced onshore supplied through long underwater power cables and may include either partial or total electrification of a single production unit, or an entire area including several units (4, 6).

Electrification of the Norwegian continental shelf is an initiative that has been debated since the mid nineties (7). By supplying the offshore facilities with onshore power, the direct emissions of burning NG in onsite gas turbines are removed, however, as the total emissions within Europe are controlled by carbon trading and

the emission scheme, some people means, in addition to that previous studies have also shown, that electrification is an unprofitable alternative with minimal effect on the total CO_2-emissions (7, 8, 9). However, most of the previous studies done on the field may have placed too much emphasis on the cost related to electrification rather than the actual effects it may have on CO_2-emissions (10).

To investigate whether electrification of the Norwegian continental shelf will reduce CO_2-emissions compared to traditional offshore power production several factors has to be accounted for: geographical perspective, timeframe, production method of onshore power and utilization of the available gas, will it come in addition to already existing power production or will it replace it (10). In most cases studied by CICERO, electrification of the Norwegian continental shelf will reduce CO_2-emissions (10). However, mostly due to cost, only a few offshore facilities are currently supplied by onshore power (7, 11).

Due to the cost related to electrification of the Norwegian continental shelf, other solutions have started to raise interest. By replacing the offshore gas turbines with a highly effective hybrid fuel cell system, CMR Prototech has suggested an alternative solution that combined with carbon capture and storage may potentially produce clean and highly efficient offshore power (CHEOP) (12, 13, 14).

As part of the CHEOP project, CMR Prototech is currently building a robust 10 kW solid oxide fuel cell (SOFC) stack ideal for offshore use that will become one of the main building blocks in future MW-scale applications (12). The goal of the project is to design a topside concept capable of producing 32 MW of electrical power at an electrical efficiency of 60% and thus replace today's offshore power generating gas turbines while simultaneously reducing the fuel consumption and thereby also the CO_2-emissions of offshore power production. By combining the process with carbon capture and storage (CCS), emissions will be almost eliminated.

The topside concept is designed to consist of 10 hybrid fuel cell modules that will deliver 3.2 MW of electrical power each, see Fig. 1.1. Each hybrid fuel cell module will consist of a SOFC module and a high temperature proton exchange membrane fuel cell (HT-PEMFC) module, where the HT-PEMFC will produce most of the electrical power, see Fig. 1.2.

To be able to replace today's offshore gas turbines, the combination of SOFC and HT-PEMFC modules in the hybrid fuel cell modules is quite essential. Offshore, NG will be utilized as fuel. As SOFCs are flexible in terms of fuel and can thereby produce electrical power from NG as well as from hydrogen, they are a crucial part of the conceptual design (14). However, due to size and weight, a pure SOFC-facility would not be suitable offshore. Combining the SOFC modules with more

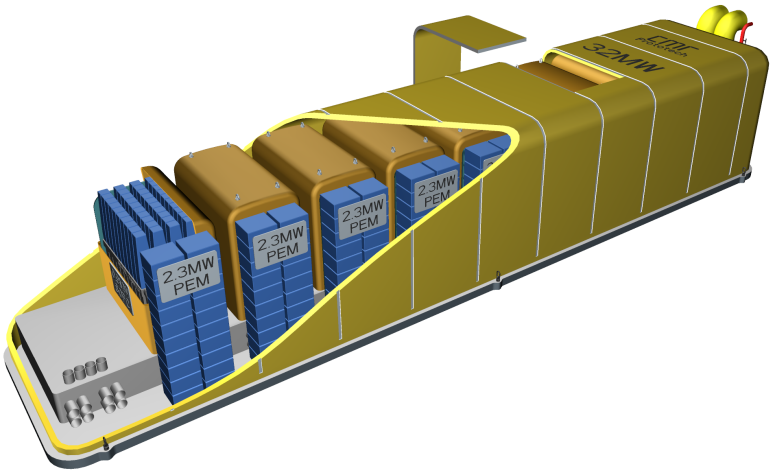

Figure 1.1: Conceptual design of CMR Prototech's 32 MW topside hybrid fuel cell system for clean and highly efficient offshore power production.

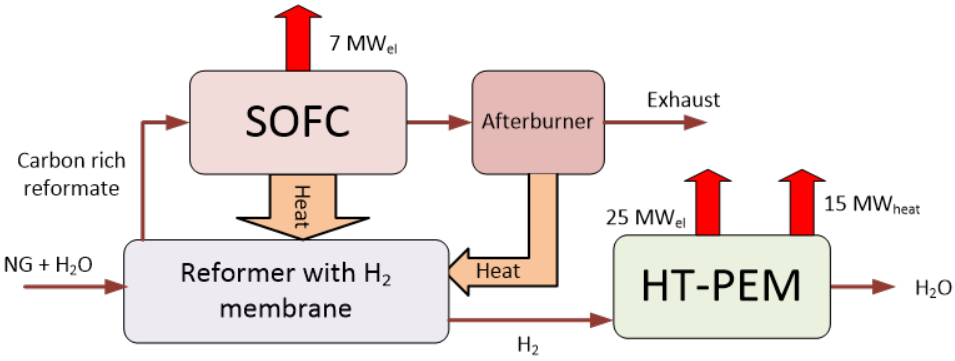

Figure 1.2: Block flow diagram of the most essential components in CMR Prototech's proposed CHEOP process.

efficient HT-PEMFC modules are therefore essential to reduce the weight of the system. However, HT-PEMFCs need hydrogen to produce power, hence, some kind of reforming process is required upstream of the hybrid fuel cell system 1.2.

CMR Prototech has developed a proposed design of a scaled-down CHEOP process that delivers 3.2 MW of electrical power at an electrical efficiency of 60% without carbon capture. In the suggested process, a membrane reactor is placed upstream of the hybrid fuel cell system to produce and separate hydrogen from the NG feed with steam (Fig. 1.2). Steam methane reforming (SMR) is a quite energy demanding process which is supplied by high quality heat from the SOFC and the afterburner, however, the presence of the membrane will probably make the reforming process less energy demanding.

In this work, a flow-sheet model of CMR Prototech's suggested CHEOP process with carbon capture was simulated in Aspen HYSYS to investigate its potential to produce clean and highly efficient power offshore. However, to be able to implement the proposed process in HYSYS, the membrane reactor of the CHEOP process was replaced by an already existing process route for syngas production and hydrogen separation as there is no specific unit operations that models the behaviour of membrane reactors in Aspen HYSYS, and to model one is outside the scope of this thesis.

Hence, based on the nominal operating conditions of CMR Prototech's proposed CHEOP process and a literature review of hydrogen production technologies, an equilibrium-based flow-sheet model of the CHEOP process with carbon capture was developed in Aspen HYSYS to investigate its potential performance in this work. Furthermore, a sensitivity analysis and a heat integration were also performed to study how the process behave and its potential for further improvements.

Chapter 2

Literature Review

2.1 Reforming of Natural Gas

The main technologies for conversion of gaseous and liquid hydrocarbons (typically fossil fuels like natural gas composed of lighter and heavier hydrocarbons) into syngas and hydrogen are steam methane reforming (SMR), partial oxidation (POX) and autothermal reforming (ATR) (15, 16, 17). The different production routes produce syngas with varying H_2/CO ratio depending on the specific feedstock, presence of catalyst and process conditions like temperature, pressure and steam-to-carbon (S/C) ratio. Among the different production routes, SMR are the oldest and most widely used due to a couple advantages compared to the other.

As POX and ATR utilize large amounts of preferably pure O_2 in the conversion process, expensive and complex oxygen separation units are required to avoid nitrogen in the product gas (16, 17). The SMR process on the other hand does not require oxygen in the conversion process, hence no expensive air separation unit is needed. The SMR process also operates at lower temperatures than the POX and ATR process, which enables cheaper materials, in addition to be the most feasible conversion process as it produces a reformate with higher H_2/CO ratio compared to the POX and ATR process (16, 17). As methane conversion, size and capital investment are important factors of the hybrid fuel cell process, the SMR reactor was selected instead of a POX or ATR reactor. The chemistry of the SMR process is further described below.

2.1.1 Steam Methane Reforming (SMR)

In SMR syngas (H_2 and CO) is produced over a Ni-based catalyst by a highly endothermic, equilibrium-limited reaction of methane and steam (Eq. 2.1) (15, 16,

17) However, this is not the only reaction taking place in the process. In addition to the SMR reaction, a water-gas shift (WGS) reaction (Eq. 2.2) displaced to the left is also present in the process yielding an overall reaction as described by Eq. 2.3 (15, 18). The WGS reaction is displayed to the left due to the high operating temperature of the SMR process.

$$\text{SMR:} \quad \mathrm{CH_4 + H_2O \rightleftharpoons CO + 3H_2} \qquad \Delta H^{\circ}_{298K} = 206\,\text{kJ/mol} \tag{2.1}$$

$$\text{WGS:} \quad \mathrm{CO + H_2O \rightleftharpoons CO_2 + H_2} \qquad \Delta H^{\circ}_{298K} = -41\,\text{kJ/mol} \tag{2.2}$$

$$\text{Overall rxn:} \quad \mathrm{CH_4 + 2H_2O \rightleftharpoons CO_2 + 4H_2} \qquad \Delta H^{\circ}_{298K} = 165\,\text{kJ/mol} \tag{2.3}$$

If CO_2 or higher hydrocarbons (C_mH_n) are present in the feed, dry reforming (Eq. 2.4) and higher hydrocarbon refroming (HHR, Eq. 2.5 and 2.6) may also take place in the reforming process (18, 19, 20).

$$\text{Dry reforming:} \quad \mathrm{CH_4 + CO_2 \rightleftharpoons 2CO + 2H_2} \qquad \Delta H^{\circ}_{298K} = 247\,\text{kJ/mol} \tag{2.4}$$

$$\text{HHR:} \quad \mathrm{C_mH_n + mH_2O \rightleftharpoons mCO + \left(m + \frac{n}{2}\right)H_2} \qquad \Delta H^{\circ}_{298K} > 0\,\text{kJ/mol} \tag{2.5}$$

$$\text{HHR:} \quad \mathrm{C_mH_n + H_2O \rightleftharpoons mCO_2 + \left(2m + \frac{n}{2}\right)H_2} \qquad \Delta H^{\circ}_{298K} > 0\,\text{kJ/mol} \tag{2.6}$$

In addition to the desired reforming reactions, a couple of unwanted reactions like CO disproportionation (Boudouard reaction, 2.7), methane cracking (Eq. 2.8) and higher hydrocarbon cracking (HHC, Eq. 2.9) may also take place in the reforming process. These reactions can be promoted by certain process conditions and lead to coke formation and catalyst deactivation in the reformer (20, 15, 18).

$$\text{Boudouard:} \quad \mathrm{2CO \rightleftharpoons C + CO_2} \qquad \Delta H^{\circ}_{298K} = -172\,\text{kJ/mol} \tag{2.7}$$

$$\text{Methane cracking:} \quad \mathrm{CH_4 \rightleftharpoons C + 2H_2} \qquad \Delta H^{\circ}_{298K} = 75\,\text{kJ/mol} \tag{2.8}$$

$$\text{HHC:} \quad \mathrm{C_mH_n \rightleftharpoons mC + \frac{n}{2}H_2} \qquad \Delta H^{\circ}_{298K} > 0\,\text{kJ/mol} \tag{2.9}$$

SMR is normally carried out at temperatures of 500-1100 °C, pressures of 20-35 atm and steam-to-carbon (S/C) ratios of 2.5-3.0, which typically produce a H_2/CO ratio of 3:1 (15, 16, 17). High conversion is promoted by high temperature, low pressure and high S/C ratio, which also reduce the risk of carbon deposition on the catalyst surface (15, 16, 17).

2.1.2 Pre-Reforming

Coke formation and carbon deposition, hence catalyst deactivation, are severe problems in steam methane reforming, especially when heavier hydrocarbons are present in the feed (15, 16, 20). One way to minimize the formation of carbon deposits on the catalyst surface in the reforming process, is to use an upstream pre-reformer (17).

In a pre-reformer, the heavier hydrocarbons of the feed breaks into CH_4, H_2 and CO in an endothermic irreversible steam reforming reaction which is followed by an equilibrium-driven exothermic methanation and water-gas-shift reaction resulting in a product mixture primarily consisting of CH_4, H_2, CO, CO_2 and H_2O (15). The overall reaction is close to be thermally neutral. Hence, pre-reformers are typically designed as adiabatic fixed-bed reforming reactors with Ni-based catalysts (15). Pre-reformer are operated at a low temperature (400-550 °C) to ensure the inhibition of the carbon formation reactions (Eq. 2.7, 2.8 and 2.9) (15, 21).

In addition to reduce the chances of catalyst deactivation of the SMR process, incorporating an adiabatic pre-reformer in the reforming process have major advantages when higher hydrocarbons are present in the feed (15):

- SMR can be operated at a lower S/C ratio, hence energy requirements of steam generation are reduced.
- Allow for greater feed temperatures to the SMR, thus reducing the size of the SMR.
- Allow feedstock flexibility.
- The Ni-catalysts in the pre-reformer can act as a sulphur trap, which will improve the lifetime of the catalysts in the SMR, WGS and SOFC.
- Allow cheaper catalysts in the SMR.
- Reduce the capital investment of the process due to the advantages above.

2.2 Water-Gas Shift (WGS) Reaction

Reforming of hydrocarbons produce synthesis gas or syngas, a mixture of H_2 and CO. The H_2 concentration of this gas usually range from 40 to 75% depending on the reforming method and conditions (22). To decrease the CO concentration and maximize the H_2 purity and yield, water-gas shift reactors are usually placed downstream of the reforming process in conventional syngas and hydrogen production processes (15, 17, 22).

In a WGS reactor CO and steam reacts to produce shifted syngas, a mixture of H_2 and CO_2. This typically happens in adiabatic fixed bed reactors over catalysts that only promotes the WGS conversion reaction (Eq. 2.2). The WGS conversion is reversible, equilibrium-limited and slightly exothermic (17, 22). Hence, low temperature favours the conversion but the reaction kinetics are favoured by higher temperatures. High S/C ratios give high CO conversion, but results also in an efficiency penalty as more water is present in the system (requires more heating) (17). The CO conversion is not affected by the total pressure as the net amount of moles is constant in the reaction (22). However, the reaction rate increases with increasing pressures (17).

Since the conversion of the WGS reaction is favoured by low temperature but its kinetics is favoured by higher temperatures, the WGS process is often divided into two separate steps for maximizing the CO conversion: first a high temperature step (HT-WGS) followed by a low temperature step (LT-WGS) (17, 22). The HT-WGS step typically operates at 310-450 °C and 10-60 bar over a $Fe_3O_4 - Cr_2O_3$ catalyst, which enables fast reaction kinetics, hence minimizes the catalyst bed volume and reduce the CO concentration down to 1-5% (17, 22). The LT-WGS step typically operates at 200-250 °C and 10-40 bar over a Cu/Zn/Al-catalyst, which favours the thermodynamics of the WGS reaction, hence enables high CO conversion and reduces the CO concentration to below 0.5% (17, 22).

The use of HT-WGS is considered to be state-of-the-art in almost every plant where H_2 is produced by the SMR process (22). The LT-WGS on the other hand, has become obsolete after implementation of pressure swing adsorption (PSA) for H_2 purification (22).

2.3 Separation of Hydrogen with Membranes

In CMR Prototech's proposed offshore process the HT-PEMFC is responsible for the majority of the electrical power generation. However, the SOFC can converts most of the components in the produced syngas. It is therefore desirable to separate the H_2 from the produced syngas as pure as possible.

Relevant technologies for H_2 separation are absorption, adsorption, cryogenic distillation/low temperature processes and membranes (17, 23). Among these, pressure swing adsorption (PSA) is the commercial available technology for H_2 separation from syngas due to its ability to produce H_2 with 98-99.9999+ mol% purity and impurity levels down to ppm levels (15, 23). However, compared to the other hydrogen separation technologies, membranes hold the potential of advantages such as (23, 24, 25, 26):

- low energy consumption
- small footprint
- low capital and operating costs
- ease of scale up
- mild process conditions
- absence of additives, hence more environmental friendly
- process flexibility
- ability for continuous separation
- possibility to combine with other separation technologies

Size, energy consumption and cost are important sustainability factors of the offshore CHP process. Moreover, a single hydrogen membrane will make a more direct comparison with the membrane reactor case.

2.3.1 Basic Membrane Theory

Membranes are selective barriers that only let certain components pass through. They are therefor ideal for separation purposes. The selective barrier divides membranes into two sections: a high pressure feed side and a low pressure permeate side. At the high pressure side feed enters. Due to the pressure difference across the membrane and its selective characteristics some of the feed permeates through the membrane while some of the feed is rejected. Permeation can actually occur in both directions but will be more favourable in the direction of low pressure (23). The amount of feed that passes through the membrane is called permeate while the rejected amount is called retentate. The permeate leaves the membrane at the low pressure side while the retentate leaves at the high pressure side. They are thereby separated. At the low pressure side an inlet stream called sweep can be utilized to enhance the transport of the desired components through the membrane.

2.4 Fuel Cells - Thermal Energy to Electrical Work

Traditional heat engines goes through a process of several step to convert the chemical energy of a fuel into power. In the first step of the process chemical energy stored in the fuel is converted to heat by combustion. In the second step of the process the thermal energy of the hot flue gas (off gas) is converted to mechanical energy directly by a gas turbine or by producing hot steam that drives a steam

turbine. In the third and last step of the process, the turbine are used to drive a generator which converts the mechanical energy of the turbines into electrical power. The ability of traditional heat engines to utilize the chemical energy stored in the fuel are limited by all these steps, and their maximum theoretical efficiency are governed by the Carnot efficiency.

A fuel cell on the other hand, is an electrochemical device that converts chemical energy stored in liquid or gaseous fuel directly into electrical energy in one single step. Through electrochemical reactions, fuel cells produce electrical energy without including the intermediate steps of combustion and mechanical energy conversion. Thus, fuel cells are not limited by the thermodynamic limitations of heat engines. They can therefore achieve higher energy efficiencies than heat engines, a feature that make fuel cells an attractive substitute of internal combustion engines in automobiles and gas turbines in power generating applications (27).

Like a battery, a fuel cell produce direct current (DC) electricity through electrochemical reactions in a single step process during isothermal conditions (27). It consists of three active components: two porous electrodes, an anode and a cathode, and an electrolyte (28). The electrochemical reactions take place at the porous electrodes, which are typically covered with catalysts to increase the rate of the electrochemical reactions (28). At the negatively charged anode, fuel is oxidized and electrons released. The electrons are forced through an external circuit that connects the anode and cathode. At the positively charged cathode, oxidants are reduced by the electrons from the anode. Sandwiched between the electrodes lies the ion-conduction electrolyte that transport charged particles between the electrodes. Depending on the fuel cell type, the charged particles can be transported from anode to cathode (PEMFC) or from cathode to anode (SOFC),

Unlike a battery, fuel cells are not discharged as electricity is produced by a constant supply of reactants - fuel and oxidant (27). Typical reactants for fuel cells are hydrogen (fuel) and oxygen (oxidant), but the purity of the reactants may vary. However, despite the purity of the reactants, fuel cells generate by-products like water and heat. Such by-products are not produced in batteries, at least not to the extent that requires any special or additional equipment (27). In fuel cells on the other hand, proper systems for continuously removal of the by-products must be in place to ensure continuous isothermal operation for ideal electric power generation. Hence, water and thermal management are key areas of efficient fuel cell design and operation (28).

Today, there are several different types of fuel cells available on the market, but since CMR Prototech's proposed hybrid fuel cell system is made up of a solid oxide fuel cell (SOFC) module and a high temperature proton exchange membrane

fuel cell (HT-PEMFC) module, only the operations of these types of fuel cells will be further described.

2.4.1 Solid Oxide Fuel Cells

In a SOFC, air is delivered to the cathode where some of the oxygen reacts with electrons from the anode and forms oxygen ions ($2O^{2-}$) by the following electrochemical reaction:

$$\text{Cathode:} \quad O_2 + e^- \rightarrow 2O^{2-} \tag{2.10}$$

While the unreacted oxygen leaves the cathode with inert nitrogen as depleted air, the reduced oxygen migrates through the ion conduction electrolyte to the anode where it reacts with the supplied fuel and produce water, electricity, heat and CO_2. Depending on the feedstock and degree of upstream processing, the composition of the fuel will vary, but it typically consists of syngas, methane, some products (H_2O and CO_2) and inerts (e.g. N_2), hence the following electrochemical reactions typically take place at the anode:

$$\text{Anode } H_2\text{:} \quad 2H_2 + 2O^{2-} \rightarrow 2H_2O + 4e^- \tag{2.11}$$

$$\text{Anode CO:} \quad 2CO + 2O^{2-} \rightarrow 2CO_2 + 4e^- \tag{2.12}$$

$$\text{Anode } CH_4\text{:} \quad CH_4 + 4O^{2-} \rightarrow CO_2 + 2H_2O + 8e^- \tag{2.13}$$

By combining the cathode reaction (Eq. 2.10) with the respective anode reactions, a SOFC produce electricity, heat and an anode off-gas, typically consisting of water, carbon dioxide, inerts and some unreacted fuel depending on its degree of fuel utilization, by the following overall conversion reactions:

$$2H_2 + O_2 \rightleftharpoons 2H_2O \qquad \Delta H^\circ_{298K} = -484\,\text{kJ/mol} \tag{2.14}$$

$$2CO + O_2 \rightleftharpoons 2CO_2 \qquad \Delta H^\circ_{298K} = -566\,\text{kJ/mol} \tag{2.15}$$

$$CH_4 + 2O_2 \rightleftharpoons CO_2 + 2H_2O \qquad \Delta H^\circ_{298K} = -802\,\text{kJ/mol} \tag{2.16}$$

In addition to the electrochemical reactions above, steam-reforming (Eq. 2.1), dry-reforming (Eq. 2.4) and the reversed WGS reaction (Eq. 2.2) may also take place at the anode due to the presence of the Ni-catalyst and the high operating temperature of the SOFC (850 °C).

2.4.2 High Temperature Proton Exchange Membrane Fuel Cells

In a HT-PEMFC, fuel (hydrogen) is delivered to the anode where it is dissociated into hydrogen ions/protons and electrons at the Pt – catalyst by the following electrochemical reaction:

$$\text{Anode:} \quad \mathrm{H_2} \rightarrow 2\mathrm{H^+} + 2\mathrm{e^-} \tag{2.17}$$

The oxidized hydrogen migrate through the electrolyte to the cathode side, while the electrons go through the electrically conductive anode electrode an forced through the the external circuit all the way to the cathode. Unreacted fuel leaves the anode as off-gas. At the cathode, air is supplied from an external gas-flow stream and some of the oxygen reacts with the electrons and the protons to produce water by the following electrochemical reaction:

$$\text{Cathode:} \quad \frac{1}{2}\mathrm{O_2} + 2\mathrm{H^+} + 2\mathrm{e^-} \rightarrow \mathrm{H_2O} \tag{2.18}$$

By combining the anode (Eq. 2.17) and the cathode (Eq. 2.18) reaction, a HT-PEMFC produce electricity, heat and water by the following overall reaction:

$$\text{Overall:} \quad \mathrm{H_2} + \frac{1}{2}\mathrm{O_2} \rightleftharpoons \mathrm{H_2O} \qquad \Delta H^{\circ}_{298K} = -286\,\text{kJ/mol} \tag{2.19}$$

Depending on the degree of fuel and oxygen utilization, the anode off-gas will contain some unreacted hydrogen and some impurities, depending on the upstream fuel processing, while the cathode exhaust will contain some unreacted oxygen and inerts (e.g. nitrogen) in addition to the produced water vapour.

Chapter 3

Conceptual Design

3.1 CMR Prototech's CHEOP Process

CMR Prototech's proposed offshore hybrid fuel cell consists of the following unit operations: a steamer, a membrane reformer, a HT-PEMFC, a SOFC, an oxygen-pump, an oxyfuel-combustor and a condenser as shown in 3.1. Desulphurized natural gas consisting of methane, ethane, propane, carbon dioxide, nitrogen and small fractions of heavier hydrocarbons like butane, pentane and hexane is used as feedstock in the process.

In the process, the natural gas feed is mixed with water, passed through a steamer and the water evaporates, which is a quite energy demanding process supplied by excess heat from the HT-PEMFC module. Subsequently the evaporated mixture is further heated, thus ready to feed a steam reformer unit. The reformer unit is assumed to be a membrane reformer operated at 750 °C and 15 bar.

In the membrane reformer natural gas and water react and produce synthesis gas, which is a quite energy demanding process supplied by heat from the oxyfuel-combustor unit (afterburner) and the SOFC module. The produced syngas consist of hydrogen, carbon monoxide, carbon dioxide, unreacted reactants (natural gas and water) and inerts like nitrogen. In the membrane reformer, most of the hydrogen is separated from the syngas due to a pressure difference across the membrane, hence two outlet streams are produced: a pure hydrogen stream and a carbon rich reformate.

Further on, the purified hydrogen is cooled, hence ready to feed the anode of a HT-PEMFC module operated at 200 °C and 1 bar. Together with preheated air fed to the cathode, hydrogen reacts to produce electricity, excess heat and water

vapour. The excess heat is supplied to the steamer for heat recovery. The anode and cathode outlet streams are kept separated. The cathode off-gas, consisting of water vapour and unreacted air, is used to preheat the inlet air while the anode outlet stream, consisting of unreacted hydrogen, is treated in an oxyfuel-combustor.

The carbon rich reformate on the other hand is passed through a valve, thus ready to feed the anode of a SOFC module operated at 850 °C and 1 bar. Together with preheated air fed to the cathode, the reformate reacts to produce electricity, excess heat, an oxygen depleted cathode outlet stream and an anode off-gas consisting of water vapour, carbon dioxide and unreacted fuel (hydrogen and carbon monoxide). While the depleted air stream is passed further on to a oxygen-pump before it is used to preheat the inlet air of the SOFC, the anode off-gas is sent to the oxyfuel-combustor and the excess heat is supplied to the membrane reformer for heat recovery.

After heat an electricity is produced in the two fuel cells, the anode products of the respective fuel cells are passed on to a oxyfuel-combustor for more heat production and further treatment. Here, unreacted fuel reacts with pure oxygen to produce more heat, which is supplied to the energy demanding membrane reformer, and an almost pure mixture of carbon dioxide and water vapour. The pure oxygen is supplied from an oxygen-pump. It is a reversed SOFC where electricity is supplied to separate oxygen from the already oxygen depleted cathode product of the SOFC. The pure oxygen outlet stream is fed to the oxyfuel-combustor while the even more oxygen depleted product is used to preheat the inlet air of the SOFC.

The resulting mixture of water vapour and carbon dioxide is sent to a dedicated condensation process to separate water and carbon dioxide. It consists of a multistage separator and compressor process with inter-cooling to achieve the required temperature, pressure and purity specifications for carbon capture and storage. After the water and carbon dioxide is separated, the purified carbon dioxide is sent to pipelines for enhanced oil recovery (EOR) or storage, while the condensed water is pressurized and recycled back to be mixed with the desulphurized natural gas feed.

3.2 Design Basis

CMR Prototech has developed a piping & instrumentation diagram (P&ID) of a 3.2 MW power generating hybrid fuel cell system that together with values from the literature, served as a design basis in this work. CMR Prototech used 6.05 mol/s of desulphurized natural gas at 15.0 bar and 0.00 °C as feedstock, hence desulphurized natural gas at the same conditions were used as feedstock in this work. The desulphurized natural gas feed was assumed to consist of methane, ethane, pro-

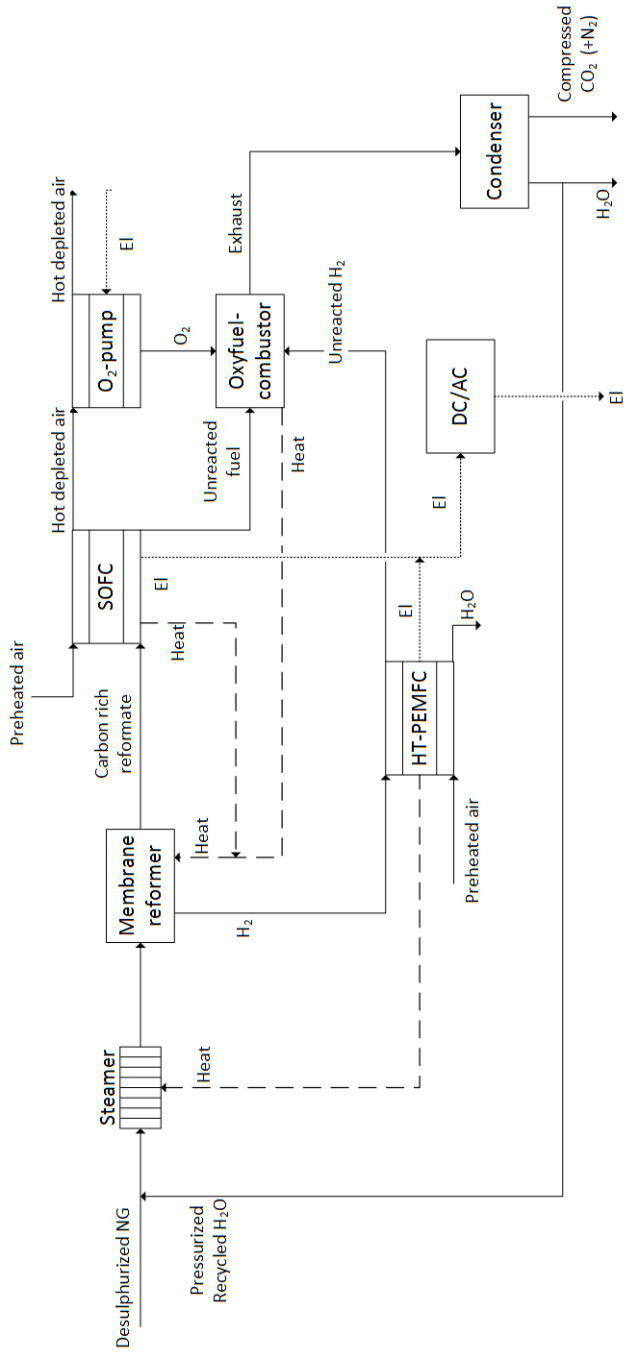

Figure 3.1: Block flow diagram of CMR Prototech's proposed hybrid fuel cell process for clean, highly efficient power production with carbon capture.

pane, carbon dioxide, nitrogen and small fractions of heavier hydrocarbons like butane, pentane and hexane represented by C_nH_{2n+2} in Table 3.1. Table 3.1 shows the composition of the desulphurized natural gas feed, which is quite comparable to the composition of desulphurized natural gas used in other literature (29).

The hybrid fuel cell system requires a certain amount of oxygen, hence air was fed to the process in addition to the desulphurized natural gas. Air was assumed to be available at a temperature and pressure of 15.0 °C and 1.00 atm, respectively. Normally, air consists of nitrogen, oxygen, argon, water vapour, carbon dioxide and trace amounts of other components like neon, helium, methane and nitrous oxide, but due to low concentration of the other gases, air is normally assumed to be a mixture only composed of nitrogen and oxygen, see Table 3.1.

Table 3.1: Design basis for the 3.2MW hybrid fuel cell system. It is based on a P&ID from CMR Prototech and other relevant literature/sources.

Design Parameter	**Value**					
Natural gas feed						
Molar composition [mol%]	CH_4: 87.8	C_2H_6: 7.63	C_3H_8: 1.32	C_nH_{2n+2}: 0.28	CO_2: 2.00	N_2: 0.96
Feed flow [mol/s]	6.05					
Pressure [bar]	15.0					
Temperature [°C]	0.00					
LHV [kJ/mol]	849					
Fuel power input, LHV [MW]	5.13					
Air feed						
Molar composition [mol%]	N_2: 79.0	O_2: 21.0				
Pressure [atm]	1.00					
Temperature [°C]	15.0					

3.3 Simulated CHEOP Process

In this work, CMR Prototech's hybrid fuel cell process with a more conventional reforming process was simulate in Aspen HYSYS. The simulated process consisted of the following unit operations: a steamer, a pre-reformer, a SMR/GHR, a H_2-selective Pd-based membrane, a hybrid fuel cell system composed of a HT-PEMFC and a SOFC, an O_2-pump, an oxyfuel-combustor and a condensation process for carbon capture, see Fig. 3.2. Table 3.2 and 3.3 show the design parameters used in simulation of the CHEOP process in this work

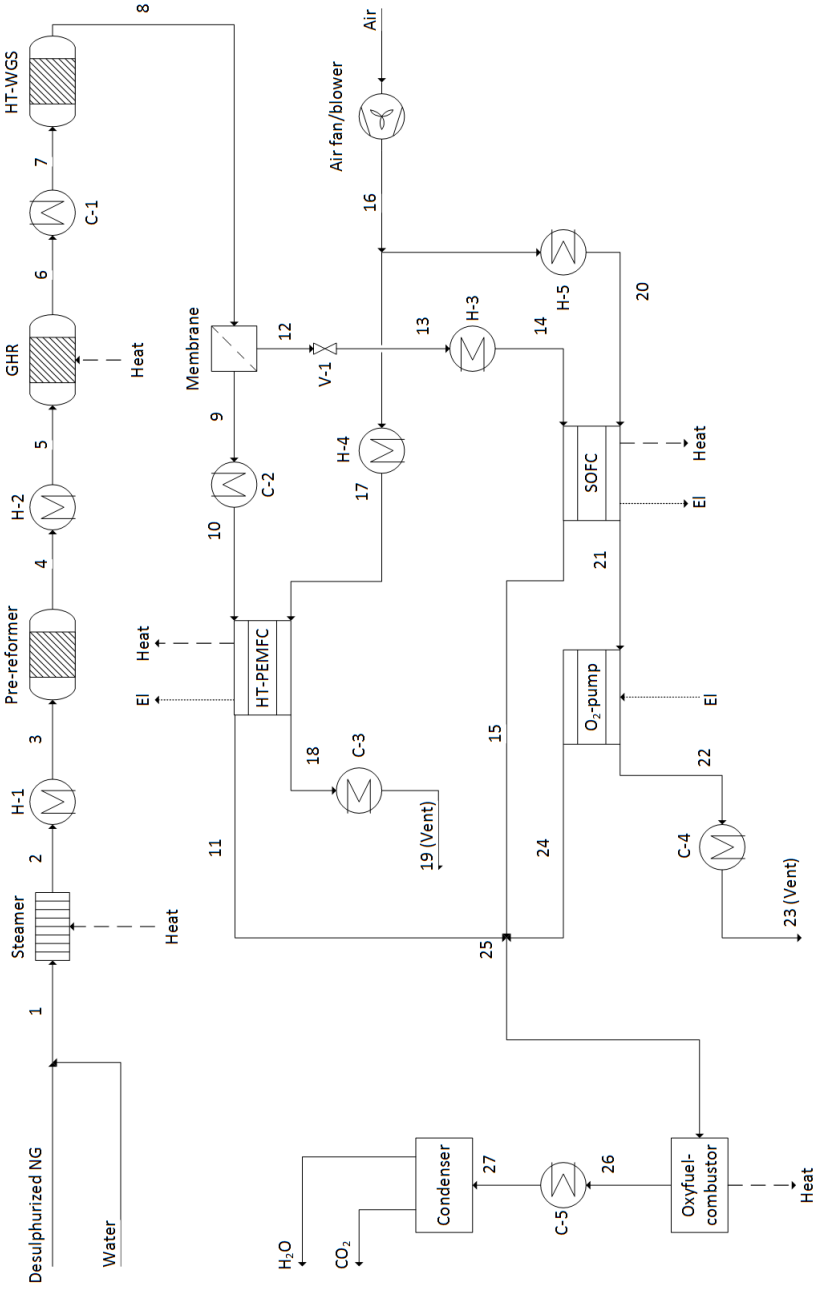

Figure 3.2: Block flow diagram of the simulated process in this work.

Table 3.2: Design parameters of the steamer, reformer, WGS reactor and Pd-membrane based on the literature and values from CMR Prototech.

Design Parameter	**Value**
Steamer	
Outlet temperature [°C]	183
Pressure drop [bar]	0.100
Pre-reformer	
Inlet temperature [°C]	400
Pressure drop [bar]	0.500
SMR/GHR	
Inlet temperature [°C]	500
Outlet temperature [°C]	750
S/C ratio [-]	2.50
Pressure drop [bar]	0.500
HT-WGS reactor	
Inlet temperature [°C]	350
Pressure drop [bar]	0.500
Pd-membrane	
Permeate pressure [bar]	1.10
Feed side pressure drop [bar]	0.100
H_2-recovery [%]	80.0
Maximum permeability [mol/(m s bar$^{0.5}$)]	$9.01*10^5$
Membrane thickness [micron]	12.0
Activation energy [J/mol]	$1.75*10^4$

Table 3.3: Design parameters of the hybrid fuel cell system and the equipment involved in the carbon capture process based on values from literature and CMR Prototech.

Design Parameter	Value
SOFC	
Feed inlet temperature [°C]	750
Air inlet temperature [°C]	700
Operating temperature [°C]	850
Operating pressure [bar]	1.00
Operating voltage [V]	0.650
Fuel utilization [%]	82.0
Oxygen utilization [%]	50.0
HT-PEMFC	
Feed inlet temperature [°C]	200
Air inlet temperature [°C]	200
Operating temperature [°C]	200
Operating pressure [bar]	1.00
Operating voltage [V]	0.750
Fuel utilization [%]	99.0
Oxygen utilization [%]	50.0
O2-pump	
Ohmic loss [V]	0.250
Oxyfuel-combustor	
Pressure drop [bar]	0.100
Oxygen utilization [%]	100
Condenser - Carbon capture process	
Outlet temperature [°C]	4.00
Outlet pressure [bar]	100
Compressor ratio	3.00
Adiabatic efficiency [%]	85.0
Outlet temperature [°C] (water)	30.0

Chapter 4

Simulation Results & Discussion

4.1 Flow Sheet Results

Table 4.1 shows the flow sheet results and process conditions of the CHP process at the nominal operating conditions given in Table 3.1, 3.2 and 3.3. The table shows, in accordance with Fig. 3.2, that to get a complete evaporation of water in the steamer, an outlet temperature of 183 °C is needed. Furthermore, they also show that all of the heavier hydrocarbons (C2+) are reformed to methane in the pre-reformer, most of the methane is reformed to CO, CO_2 and H_2 in the GHR and that most of the produced CO is shifted to H_2 in the HT-WGS reactor as expected. Higher conversion of CO can be achieved by adding more water to the HT-WGS reactor, however, this additional amount of water has to be knocked out of the HT-PEMFC exhaust, stream 19 in Table 4.1, as the water product stream is just big enough to supply the water feed, notably at the nominal operating conditions. Due to a hydrogen recovery of 80.0% in the Pd-membrane, most of the produced H_2 is sent to the HT-PEMFC while the rest is passed to the SOFC with the rest of the reformate.

In the fuel cells, the fuel reacts with oxygen and produce electricity and heat in addition to byproducts like water and CO_2 (only in the SOFC), but due to incomplete combustion some H_2 and CO (only in the SOFC) leave the cells unreacted as shown in Table 4.1. The unreacted fuel are combusted in the oxyfuel-combustor producing a product mixture of CO_2 and water with small fractions of nitrogen. The presence of nitrogen in the product is due to the nitrogen content in the natural gas feedstock and not the process route itself as the oxyfuel-combustor utilize pure oxygen from the oxygen-pump and the air is never mixed with the fuel in the fuel cells.

Table 4.1 and Fig. 3.2 show that the product mixture from the oxyfuel-combustor is sent to a condenser where water is knocked out of the mixture producing a CO_2 product stream for storage at 4 °C and 100 bar, which contains some nitrogen, and a water product stream containing some CO_2 for recycling. Due to convergence problems, the recycle loop was not closed during the simulations. It is therefore worth to notice the difference in composition and pressure of the water feed and the water product in Table 4.1. As the produced water contains some CO_2, the actual recycled stream of the process will be a little bit bigger than the given water feed. Dry reforming (Eq. 2.4) is also more energy consuming than steam reforming (Eq. 2.1). In addition, the pressure of the water product is lower than the pressure of the water feed. Hence, the actual energy demand of the GHR and the net electrical power output of the plant will be bigger and lower than the respective values given in Table 4.3. However, the CO_2 content of the recycled stream is very small and it is not particularly energy demanding to pressurize the liquid water stream with a pump. Thus, not closing the recycle loop is assumed to have negligible impact on the energy demand of the GHR and the net electrical power output of the process.

4.2 Performance of The Hybrid Fuel Cell System

Table 4.2 shows the performance of the hybrid fuel cell system of the CHP process at the nominal operating conditions. With a hydrogen recovery of 80.0%, which ensures that almost as much fuel is delivered to the HT-PEMFC as to the SOFC, see stream 9 and 12 in Table 4.1, the HT-PEMFC has the biggest oxygen and air consumption of the two fuel cells due to a higher fuel utilization (Table 3.3). Table 4.2 also shows that more than twice the amount of fuel is transported through the HT-PEMFC than through the SOFC. Hence, the HT-PEMFC produce a higher current than the SOFC even though only 2 electrons are involved in the electrochemical reactions of the HT-PEMFC compared to 4 electrons in the SOFC. With both higher current and operating cell voltage, the HT-PEMFC gets a bigger electrical power output in addition to a better electrical efficiency than the SOFC.

From Table 4.2 it can also be seen that the HT-PEMFC has a greater total power output than the SOFC. Table 4.1 shows that the inlet temperatures of the HT-PEMFC are equal to the operating temperature of the cell, while the SOFC has a significant difference between inlet and operating temperatures. Some of the energy produced in the SOFC is therefore used to heat the feed streams. Hence, due to its design, the HT-PEMFC has a bigger total power output than the SOFC even though the SOFC has a slightly bigger fuel supply. Furthermore, as there is no internal reforming in the HT-PEMFC and the other heat sinks of the cell are negligible, again due to its design, the HT-PEMFC also produce more heat available for heat recovery than the SOFC. However, this heat is of lower quality than the

Table 4.1: Thermodynamic conditions and chemical compositions of the CHP process at nominal operating conditions where C2+ represents the hydrocarbons heavier than methane. The stream names correspond to the nomenclature of Fig. 3.2.

Stream	T [°C]	P [bar]	n [kmol/h]	Composition [mol%]							
				CH_4	CO	CO_2	C2+	H_2	H_2O	N_2	O_2
NG	0.00	15.0	21.8	87.8	-	2.00	9.23	-	-	0.960	-
Water	30.0	15.0	60.0	-	-	-	-	-	100	-	-
Air	15.0	1.01	392	-	-	-	-	-	-	79.0	21.0
1	25.0	15.0	81.8	23.4	-	0.533	2.46	-	73.4	0.256	-
2	183	14.9	81.8	23.4	-	0.533	2.46	-	73.4	0.256	-
3	400	14.8	81.8	23.4	-	0.533	2.46	-	73.4	0.256	-
4	366	14.3	85.0	25.9	$8.90 * 10^{-3}$	2.37	-	4.59	66.9	0.246	-
5	500	14.2	85.0	25.9	$8.90 * 10^{-3}$	2.37	-	4.59	66.9	0.246	-
6	750	13.7	112	7.73	6.89	6.88	-	44.4	33.9	0.187	-
7	350	13.6	112	7.73	6.89	6.88	-	44.4	33.9	0.187	-
8	406	13.1	112	7.73	1.72	12.0	-	49.6	28.7	0.187	-
9	408	1.10	44.3	-	-	-	-	100	-	-	-
10	200	1.00	44.3	-	-	-	-	100	-	-	-
11	200	1.00	0.443	-	-	-	-	100	-	-	-
12	406	13.0	67.3	12.8	2.85	20.0	-	16.5	47.6	0.310	-
13	402	1.10	67.3	12.8	2.85	20.0	-	16.5	47.6	0.310	-
14	750	1.00	67.3	12.8	2.85	20.0	-	16.5	47.6	0.310	-
15	850	1.00	84.6	-	3.05	25.3	-	7.06	64.3	0.247	-
16	23.1	1.10	392	-	-	-	-	-	-	79.0	21.0
17	200	1.00	207	-	-	-	-	-	-	79.0	21.0
18	200	1.00	229	-	-	-	-	0.192	19.0	71.4	9.48
19	56.0	0.900	229	-	-	-	-	0.192	19.0	71.4	9.48
20	700	1.00	186	-	-	-	-	-	-	79.0	21.0
21	850	1.00	166	-	-	-	-	-	-	88.3	11.7
22	850	1.00	162	-	-	-	-	-	-	90.7	9.27
23	81.4	0.900	162	-	-	-	-	-	-	90.7	9.27
24	850	1.00	4.50	-	-	-	-	-	-	-	100
25	848	1.00	89.5	-	2.88	23.9	-	7.16	60.8	0.233	5.02
26	550	0.700	85.0	-	-	28.2	-	-	71.5	0.246	-
27	200	0.600	85.0	-	-	28.2	-	-	71.5	0.246	-
H_2O	30.0	0.500	60.8	-	-	$2.40 * 10^{-2}$	-	-	100	-	-
CO_2	4.00	100	24.2	-	-	99.1	-	-	-	0.864	-

heat recovered from the SOFC and can only be used in the steamer and other low quality sinks of the process while the heat from the SOFC can be utilized to drive the endothermic reactions of the GHR.

Table 4.2: Performance of the hybrid fuel cell system the CHP process at nominal operating conditions.

Fuel cell performance	SOFC	HT-PEMFC
O_2 consumption [kmol/h]	19.5	21.7
Air consumption [kmol/h]	186	207
H_2 consumption [kmol/h]	-	43.9
Current [kA]	2090	2350
Electrical power output [kW]	1360	1760
Total power output [kW]	2660	2940
Heat consumption internal reforming [kW]	554	-
Heat consumption anode off-gas [kW]	-	-
Heat consumption cathode off-gas [kW]	229	0.207
Heat available for heat recovery [kW]	520	1170
Electrical efficiency (LHV basis) [%]	51.0	60.0

4.3 Plant Performance of The CHP Process

Table 4.3 shows the plant performance of the CHP process at the nominal operating conditions. At these conditions, the CHP process has a methane conversion of 60.7%, which requires 1060 kW of high quality heat in the GHR. Furthermore, a total H_2 production of 55.4 kmol/h is achieved at the nominal operating conditions. With a hydrogen recovery of 80.0% in the Pd-membrane, 80.0% of the total hydrogen production is supplied to the HT-PEMFC, which requires a total membrane area of 41.6 m^2.

A methane conversion of 60.7% is low compared to conventional SMR plants for syngas production in the literature, however, these plants tend to operate at much higher temperatures than the CHP process. Even though the CHP process operates at a quite favourable pressure and S/C ratio, it is not enough to compensate for the low operating temperature. Nevertheless, the outlet temperature of the GHR was chosen to ensure that the process was not becoming too energy-intensive and thereby not accomplish one of its most important criteria: to be self-supplied with heat.

From Table 4.3 it can also be seen that with an electrical power production in the SOFC and the HT-PEMFC as shown in Table 4.2 and with an electrical power

Table 4.3: Plant performance of the CHP process at nominal operating conditions.

Parameter	Value
Required heat GHR [kW]	1060
CH_4 conversion [%]	60.7
H_2 production [kmol/h]	55.4
Membrane area [m^2]	41.6
Power input of NG feedstock (LHV basis) [kW]	5130
Total electrical power output [kW]	3120
Air fan/blower [kW]	25.5
Condensation process [kW]	107
Oxygen-pump [kW]	95.6
Total electrical power consumption [kW]	228
Net electrical power output [kW]	2890
Electrical plant efficiency (LHV basis) [%]	56.4

consumption as shown in Table 4.3, the net electrical power production of the CHP process is 2890 kW, which gives an electrical efficiency of 56.4% at the nominal operating conditions. Although the electrical efficiency is quite good, as the Carnot efficiency is included, the results of the CHP process are a bit lower than desired: a net electrical power output of 3.2 MW with an electrical efficiency of 60.0% (14). However, it is important to remember that the results from Table 4.3 include the power consumption of the capture process, which is the biggest contributor to the total electrical power consumption in the process, while the desired/expected results from CMR Prototech do not include the power consumption of the capture process. Hence, the CHP process performs quite well at the nominal operating conditions, but there may be a potential for further improvements.

Since the HT-PEMFC has a higher electrical efficiency than the SOFC, a higher power production and a better electrical efficiency can be achieved in the CHP process by supplying more fuel to the HT-PEMFC. This can be done either by increasing the hydrogen recovery of the membrane or by increasing the overall hydrogen production in the process. Nevertheless, due to the trade-off of the CHP process, the process cannot be improved without knowing if the heat criteria of the process is achieved. Hence, a quick heat integration of the CHP process at the nominal operating conditions was performed before the sensitivity analysis was conducted.

4.4 Quick Heat Integration

Before the process can be further improved it is important to know if there is sufficient with heat produced in the process. Table 4.4 and 4.5 show the cold and hot streams and components of the CHP process with their respective inlet and outlet temperatures and the amount that needs to be cooled or heated. As expected, the tables show that the steamer, the GHR and the SOFC air feed are the most energy demanding components/streams while the HT-PEMFC, the SOFC, the oxyfuel-combustor and the depleted air from the O_2-pump are the biggest energy sources of the process. Furthermore, it can be seen that the HT-PEMFC produce more than enough heat and operates at a high enough temperature to supply the energy demand of the steamer. The pre-reformer feed and the GHR feed can be supplied by the HT-PEMFC feed and the condenser feed. Together, the SOFC and the oxyfuel-combustor deliver enough heat at high enough temperature to supply the GHR. These components also need to supply the SOFC feed, at least the last part, but most of the SOFC feed can be covered by the WGS feed such that most of the high quality heat produced by the SOFC and the oxyfuel-combustor can be utilized in the GHR. The HT-PEMFC and SOFC air feeds are covered by the cathode off-gas of the HT-PEMFC and the depleted air form the O_2-pump, respectively. Hence, there is enough heat available in the CHP process for it to be self-supplied.

Table 4.4: Cold streams and components that require heating in the CHP process at nominal operating conditions. The nomenclature corresponds to that of Fig. 3.2.

Cold streams/components	Q [kW]	T_{in} [°C]	T_{out} [°C]	n [kmol/h]
Steamer	860	25.0	183	81.8
Pre-reformer feed (H-1)	207	183	400	81.8
GHR feed (H-2)	138	366	500	85.0
GHR	1060	500	750	85.0
SOFC feed (H-3)	282	402	750	67.3
HT-PEMFC air feed (H-4)	302	23.1	200	207
SOFC air feed (H-5)	1090	23.1	700	186

4.5 Sensitivity Analysis

From the above results, it can be seen that the trade-off between heat and power production in the GHR process is shifted too far against heat at the nominal operating conditions, resulting in a lower electrical efficiency and power production than desired. To shift the process towards a higher power production, more fuel has to be sent to the HT-PEMFC as it has the highest electrical efficiency of the two fuel cells in the hybrid fuel cell system. This can be achieved either by in-

Table 4.5: Hot streams and components that require cooling in the CHP process at nominal operating conditions. The nomenclature corresponds to that of Fig. 3.2.

Hot streams/components	Q [kW]	T_{in} [°C]	T_{out} [°C]	n [kmol/h]	T_{op} [°C]
WGS feed (C-1)	465	750	350	112	
HT-PEMFC feed (C-2)	74.7	408	200	44.3	
HT-PEMFC	1170				200
SOFC	520				850
HT-PEMFC cathode off-gas (C-3)	302	200	56.0	229	
Depleted air from O_2-pump (C-4)	1090	850	81.4	162	
Oxyfuel-combustor	958	848	550	89.5	
Condenser feed (C-5)	331	550	200	85.0	

creasing the hydrogen production of the process, which is achieved by a lower operating pressure, a higher S/C ratio or a higher operating temperature in the GHR, or by increasing the membrane area and thereby the hydrogen recovery of the Pd-membrane. A sensitivity analysis was therefore performed on these variables to see how they affect the trade-off and which one that has the biggest potential to improve the power production of the process.

4.5.1 Natural Gas Feed Pressure

There can be huge variations in the natural gas feed pressure of the CHP process depending on the offshore location. As the pressure have a significant impact on the equilibrium reactions in the reformer, it affects the performance of process. It was therefore of interest to study how variations in the natural gas feed pressure affect the CHP process.

The natural gas feed pressure was varied between 10.0 and 30.0 bar, passing through the nominal condition at 15.0 bar. Fig. 4.1 shows that the outlet temperature of the steamer increases with an increasing pressure, while Fig. 4.2 shows that there is a slightly increase in the energy demand of the steamer. Pressurized fluids evaporate at higher temperatures, hence more energy is required to evaporate such fluids. Therefore, as the pressure of the fuel and water mixture increase, a higher outlet temperature and more energy is required in the steamer.

From Fig. 4.3 it can also be seen that an increasing pressure has a negative effect on the methane conversion of the GHR, which also leads to a lower energy demand in the reformer (Fig. 4.2). In the GHR, methane and water react to CO_2 and H_2 by the overall equilibrium reaction described by Eq. 2.3, which shows that higher pressures shift the equilibrium towards the reactants. Furthermore, a lower methane conversion means a lower hydrogen production. It becomes therefore easier to operate the membrane at 80.0% recovery, hence the membrane area decrease with

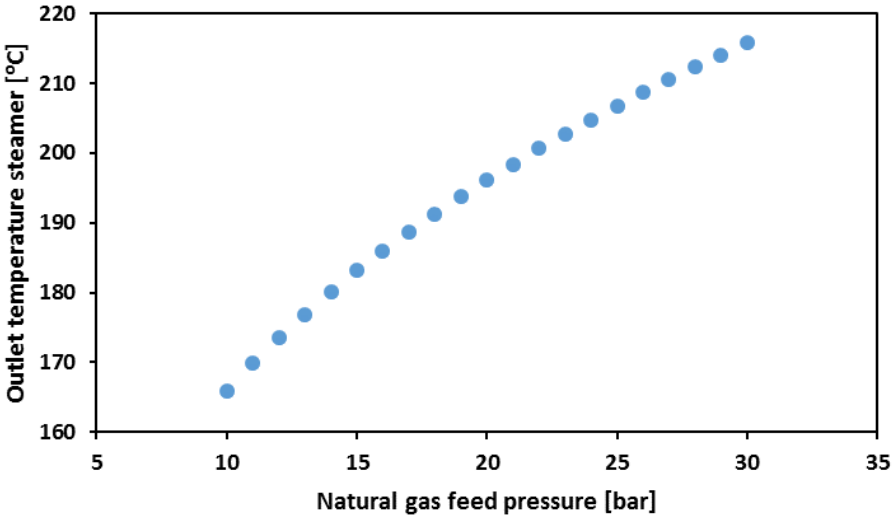

Figure 4.1: Outlet temperature of the steamer in the CHP process plotted against the natural gas feed pressure. The rest of the variables were kept constant at the nominal operating conditions.

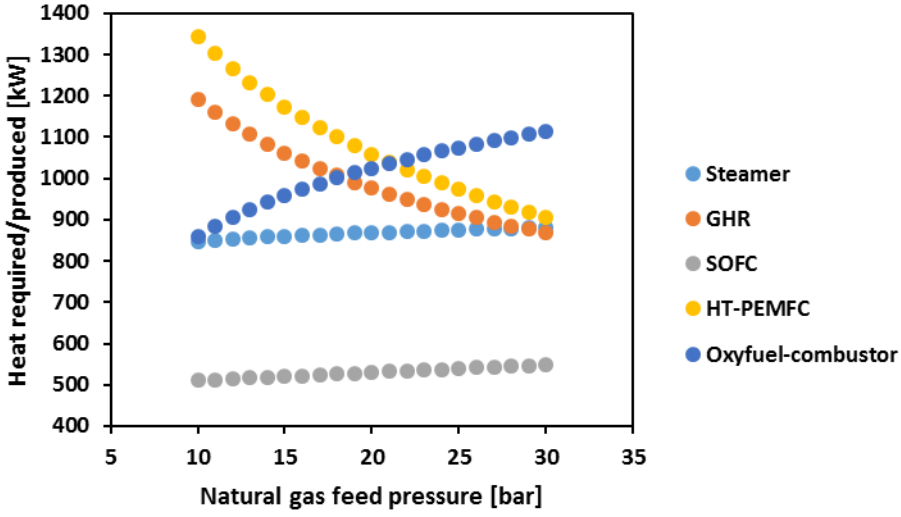

Figure 4.2: Required and produced heat of the different components in the CHP process plotted against the natural gas feed pressure. The rest of the variables were kept constant at the nominal operating conditions.

an increasing pressure (Fig. 4.4) even though higher pressures actually favour the separation.

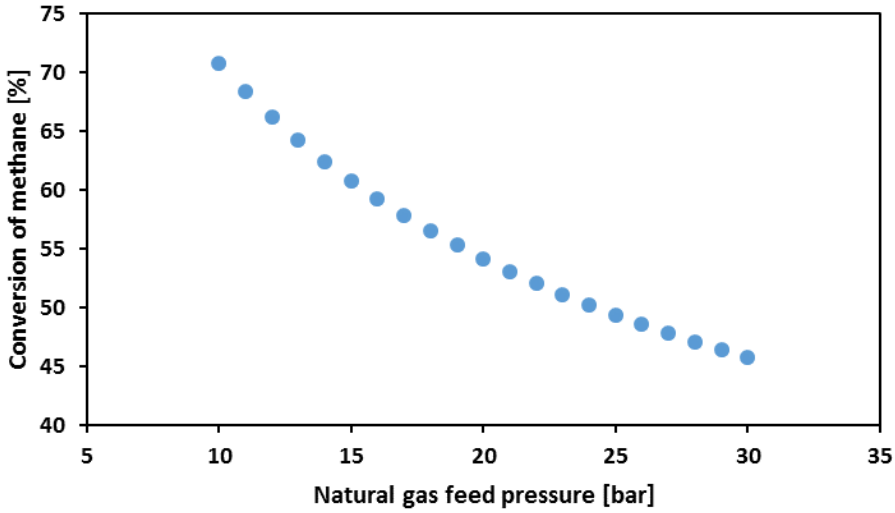

Figure 4.3: Conversion of methane in the CHP process plotted against the natural gas feed pressure. The rest of the variables were kept constant at the nominal operating conditions.

As less H_2 is transported across the membrane at higher pressures, more and more of the fuel is passed to the SOFC rather than the HT-PEMFC as the pressure increase (Fig. 4.5). An increasing pressure results therefore in a higher heat production in the SOFC and the oxyfuel-combustor, and a higher electrical production in the SOFC, while the heat and electrical production of the HT-PEMFC decrease (Fig. 4.2 and 4.6). Since the HT-PEMFC have a higher electrical efficiency than the SOFC, the total and thereby the net electrical power production of the process decrease with an increasing natural gas feed pressure.

The above results show that the trade-off between heat and electrical power generation in the CHP process can be shifted towards a higher electrical production by decreasing the natural gas feed pressure. Lower pressures will also make the cold streams of the process less energy demanding to heat up. Hence, if the natural gas feed pressure is high it should be considered to place a gas turbine upstream of the steamer. In addition to lower the pressure it might also contribute to the electrical efficiency of the process depending on the pressure and size of the natural gas it handles. On the other hand, low feed pressures increase the size of the needed membrane area, the volume of the gas in the process and thus the size of the equipment throughout the process, which is not desirable when cost is considered.

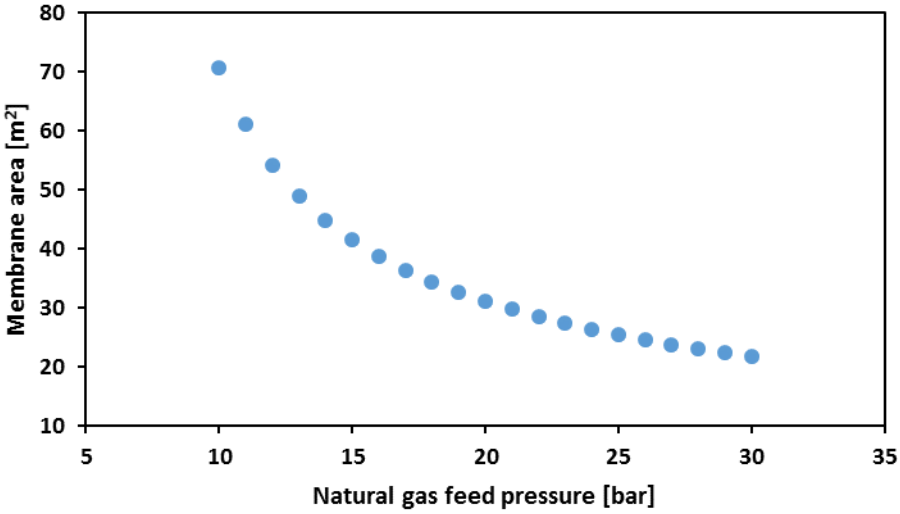

Figure 4.4: Membrane area of the Pd-membrane in the CHP process plotted against the natural gas feed pressure. The rest of the variables were kept constant at the nominal operating conditions.

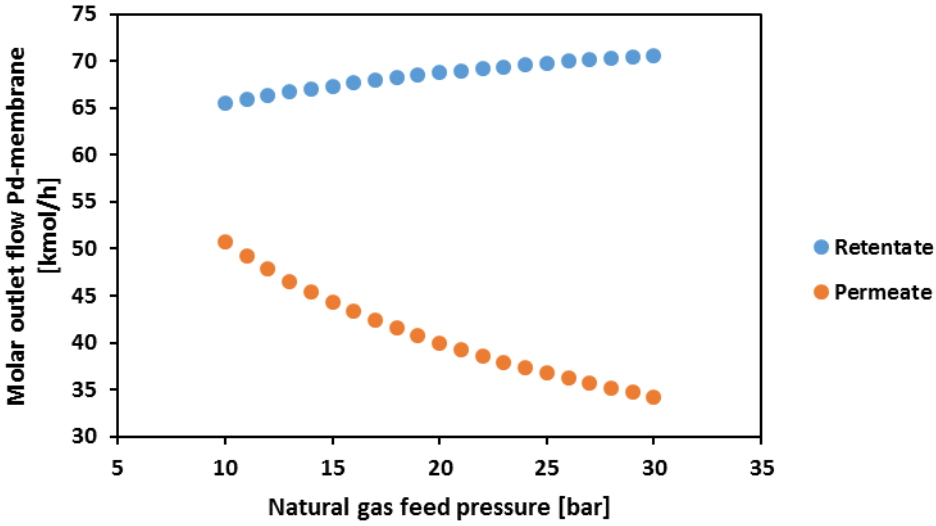

Figure 4.5: Molar outlet flow of the Pd-membrane in the CHP process plotted against the natural gas feed pressure. The rest of the variables were kept constant at the nominal operating conditions.

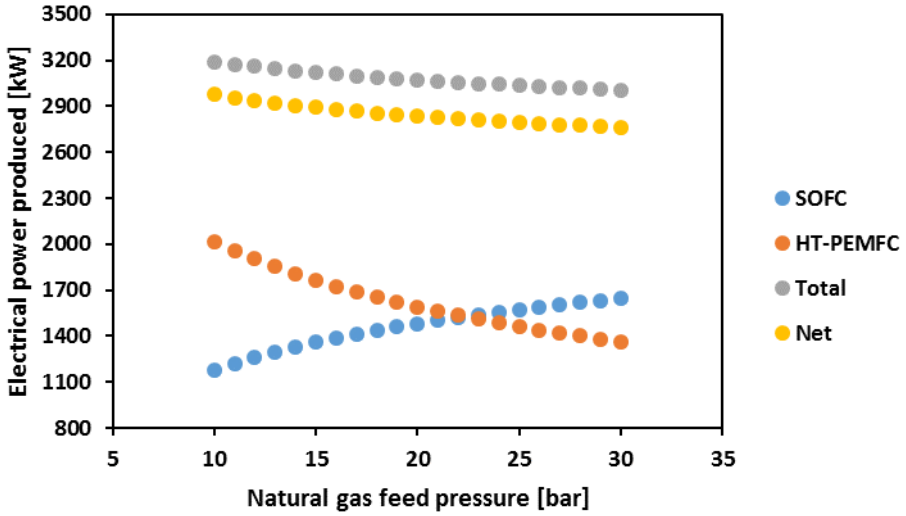

Figure 4.6: Electrical power produced by the two fuel cells in the CHP process plotted against the natural gas feed pressure. The rest of the variables were kept constant at the nominal operating conditions.

4.5.2 S/C Ratio

Since water is produced in the process, the S/C ratio is easy to control by recirculating more or less water. However, at a certain S/C ratio the amount of water needed in the feed becomes bigger than what the condenser can deliver. At such ratios, water has to be knocked out of the HT-PEMFC cathode off-gas to supply the feed, which will require an additional cooler and separator in the process. Furthermore, sufficient of water is needed in the reformer to prevent coke formation and catalyst deactivation. Finally, the S/C ratio also affect the equilibrium reactions of the reformer. It was therefore of interest to study how variations in the S/C ratio affect the CHP process.

The S/C ratio was varied between 1.50 and 3.50 where 2.50 represents the nominal case. As shown in Fig. 4.7, the outlet temperature of the steamer increases with an increasing S/C ratio as more water becomes present, however, the effect is more moderate than that of an increasing pressure shown in Fig. 4.1. Furthermore, an increasing S/C ratio also increases the energy demand of the steamer (Fig. 4.8), and it has a greater impact than an increasing pressure as more water needs to be evaporated.

Due to the presence of more water in the reformer, the equilibrium reactions of the

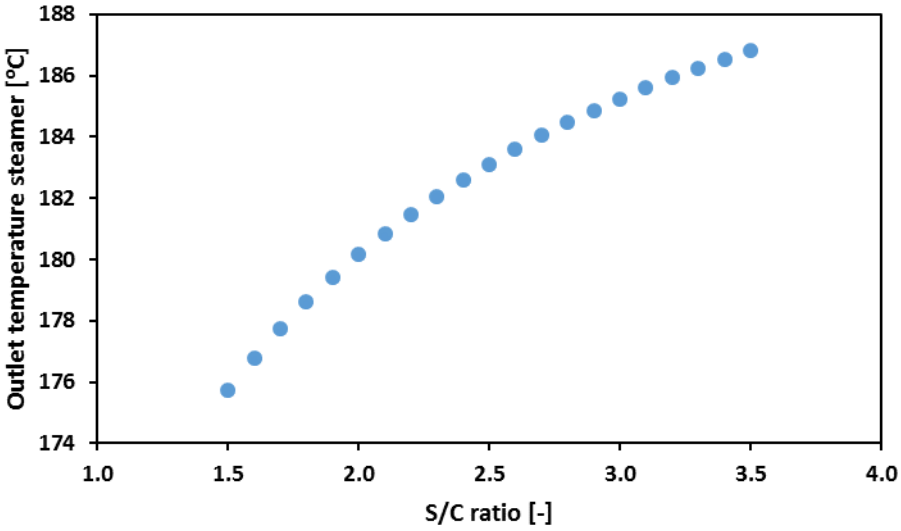

Figure 4.7: Outlet temperature of the steamer in the CHP process plotted against the S/C ratio. The rest of the variables were kept constant at the nominal operating conditions.

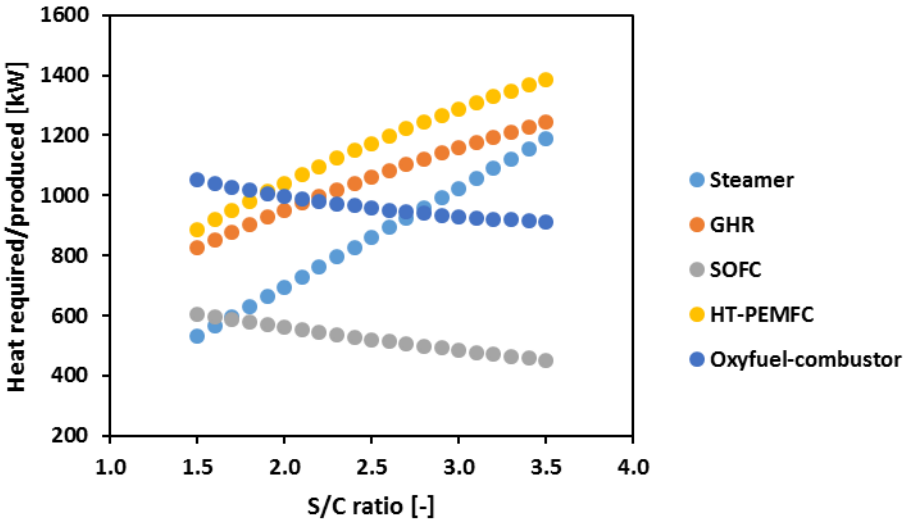

Figure 4.8: Required and produced heat of the different components in the CHP process plotted against the S/C ratio. The rest of the variables were kept constant at the nominal operating conditions.

reformer are shifted towards the products as the S/C ratio increases. Hence, the methane conversion, the hydrogen production and the energy demand of the GHR all increase at higher S/C ratios (Fig. 4.8 and 4.9). Furthermore, Fig. 4.10 shows that also higher membrane areas are needed as the S/C ratio increases. As the S/C ratio increases, the partial pressure difference across the membrane is reduced, hence, the separation of hydrogen becomes more difficult and a higher membrane area is needed to recover 80.0% of the produced hydrogen.

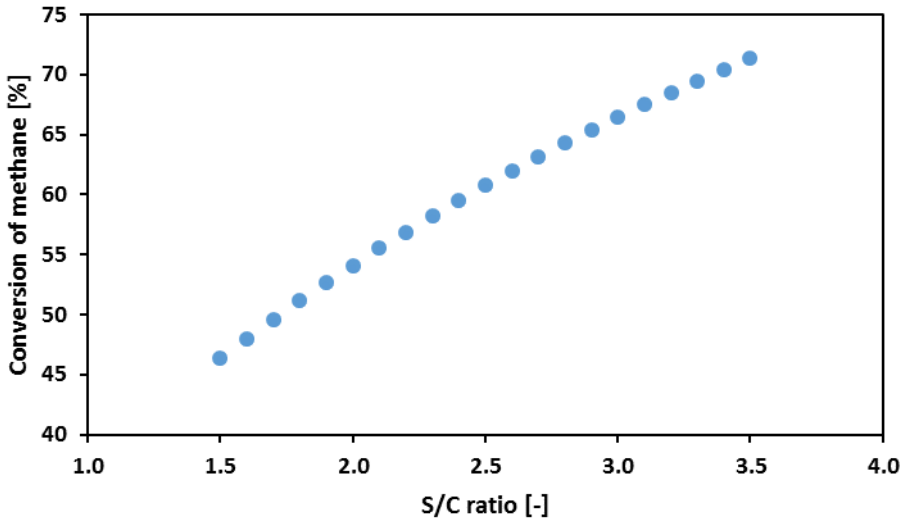

Figure 4.9: Conversion of methane in the CHP process plotted against the S/C ratio. The rest of the variables were kept constant at the nominal operating conditions.

Since the hydrogen production increases and the hydrogen recovery is kept constant with an increasing S/C ratio, the permeate flow of the Pd-membrane increases with an increasing S/C ratio and more of the fuel is supplied to the HT-PEMFC in the process (Fig. 4.11). From the figure the total retentate flow, which is passed to the SOFC, also increases, but this is only because more water is present in the process. Hence, less fuel is passed to the SOFC with an increasing S/C ratio. As more of the fuel is passed to the HT-PEMFC, the heat and electrical production of the HT-PEMFC increase, the heat and electrical production of the SOFC decrease, the oxyfuel-combustor produces less heat and the net electrical power production of the process increases with an increasing S/C ratio (Fig. 4.8 and 4.12).

From the above results it can be seen that the trade-off between heat and electrical power generation can be shifted towards a higher electrical power production by increasing the S/C ratio of the CHP process. However, greater S/C ratios will

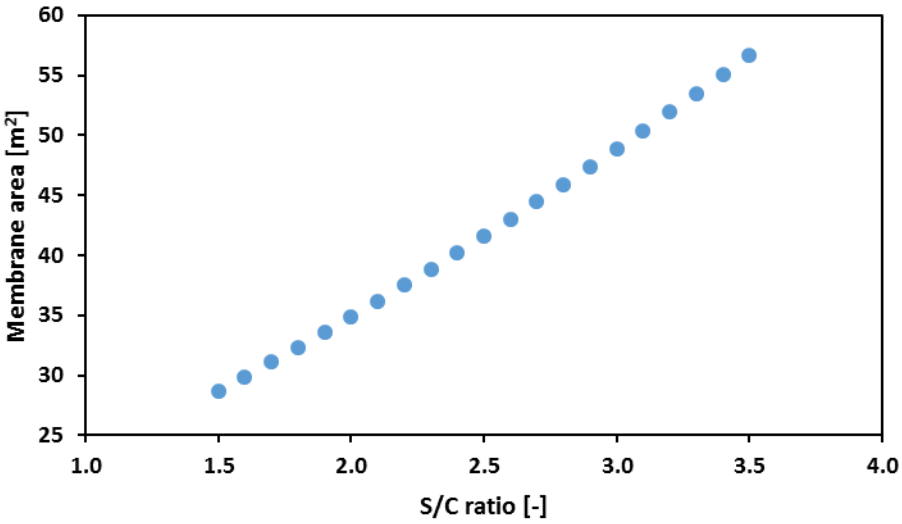

Figure 4.10: Membrane area of the Pd-membrane in the CHP process plotted against the S/C ratio. The rest of the variables were kept constant at the nominal operating conditions.

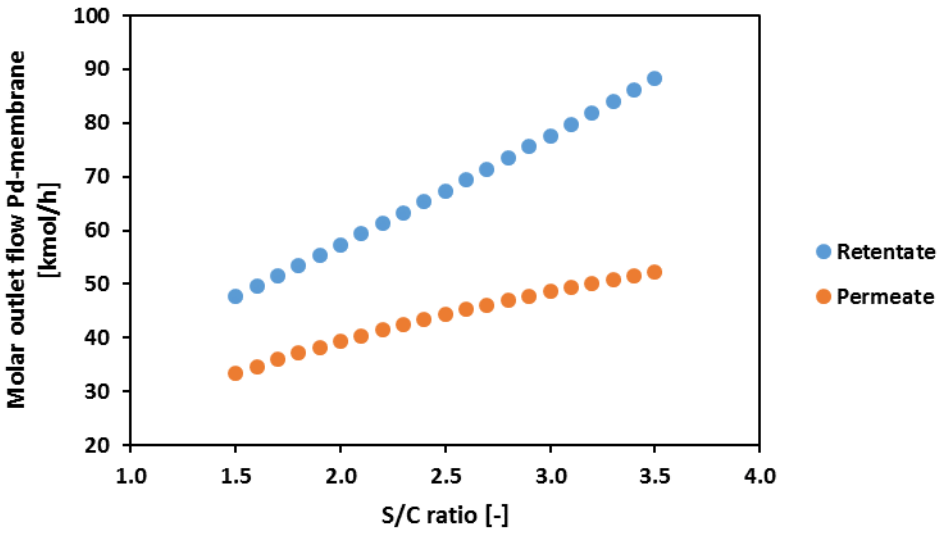

Figure 4.11: Molar outlet flow of the Pd-membrane in the CHP process plotted against the S/C ratio. The rest of the variables were kept constant at the nominal operating conditions.

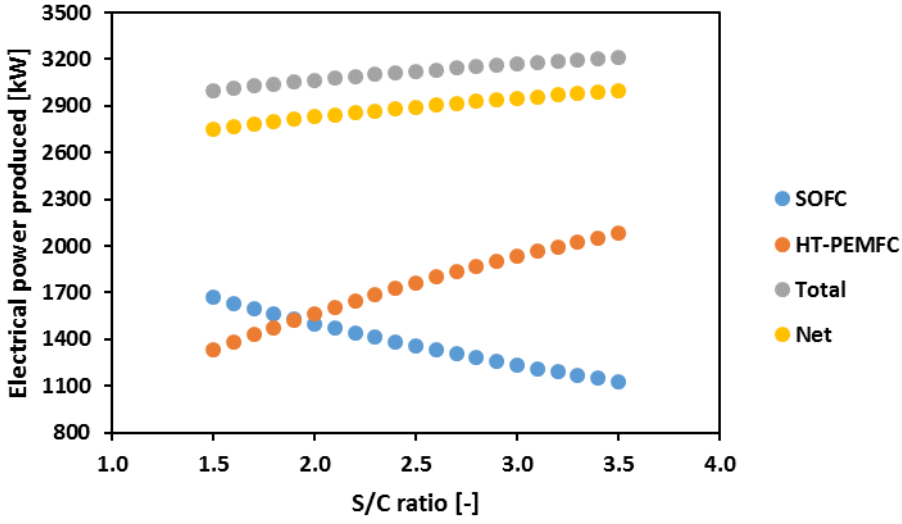

Figure 4.12: Electrical power produced by the two fuel cells in the CHP process plotted against the S/C ratio. The rest of the variables were kept constant at the nominal operating conditions.

also increase the energy demand of the steamer, the GHR and other heaters in the process, in addition to increase the membrane area and the size of the equipment throughout the process as more water becomes present in the process. Furthermore, higher S/C ratios than 2.50 will also require water from the cathode off-gas of the HT-PEMFC as the condenser will not be able to deliver enough water to supply the feed. An increased S/C ratio will therefore not only increase the electrical efficiency of the process, but also contribute to greater costs related to it.

4.5.3 Outlet Temperature of The GHR

Steam-methane reforming is a very energy demanding process as the reactions taking place in the reformer have a highly endothermic nature. To ensure that the CHP process was self-supplied at its nominal operating conditions, a moderate outlet temperature of 750 °C was chosen. Due to its behaviour, a higher outlet temperature may be favourable for the process. It was therefore of interest to see how different outlet temperatures of the GHR affect the performance of the CHP process.

The outlet temperature of the GHR was varied between 650 °C and 1050 °C, where 750 °C represents the nominal value. Due to the endothermic nature of the overall reforming reaction (Eq. 2.3), an increase in the outlet temperature of the reformer

has a positive effect on the methane conversion of the process, which can be seen from Fig. 4.13. The figure shows that the methane conversion increases quite rapidly with increasing outlet temperature until about 880 °C, where approximately 90% of the methane has been converted. After 880 °C the curve flattens out as it becomes harder and harder to covert the remaining methane due to lower methane concentrations in the reformer.

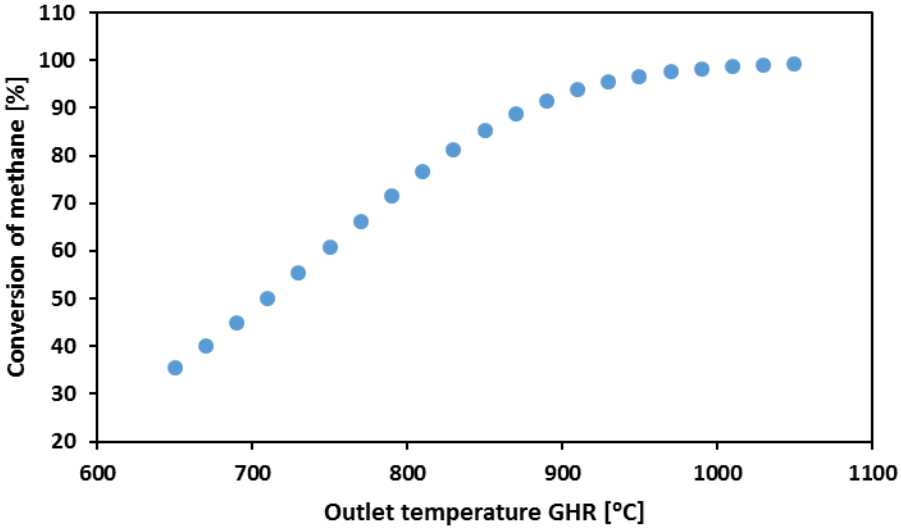

Figure 4.13: Conversion of methane in the CHP process plotted against the outlet temperature of the GHR. The rest of the variables were kept constant at the nominal operating conditions.

As the methane conversion increases with an increasing outlet temperature, the energy demand of the GHR also increases, see Fig. 4.14. In addition to a more energy demanding GHR, an increasing methane conversion also leads to a higher hydrogen production in the process. With a higher hydrogen concentration in the reformate, the hydrogen flux across the Pd-membrane increases, which results in a smaller membrane area and a bigger permeate flow when the hydrogen recovery is kept constant, see Fig. 4.15 and 4.16, respectively. As the permeate flow increases, more and more of the fuel is passed to the HT-PEMFC with an increasing outlet temperature of the GHR.

In addition to show the increasing energy demand of the GHR, Fig. 4.14 shows the behaviour of the heat production of the HT-PEMFC, the oxyfuel-combustor and the SOFC as more and more of the fuel is passed to the HT-PEMFC with an increasing outlet temperature. As expected, the heat production of the HT-PEMFC

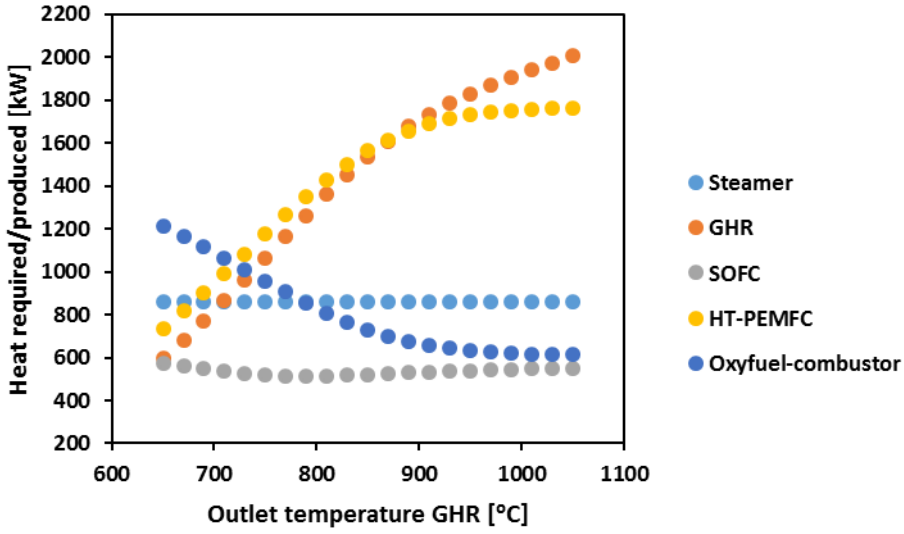

Figure 4.14: Required and produced heat of the different components in the CHP process plotted against the outlet temperature of the GHR. The rest of the variables were kept constant at the nominal operating conditions.

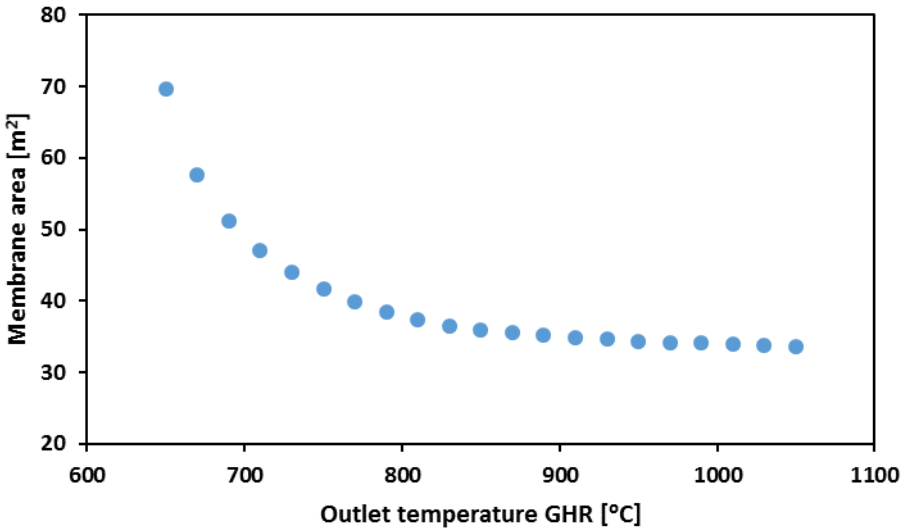

Figure 4.15: Membrane area of the Pd-membrane in the CHP process plotted against the outlet temperature of the GHR. The rest of the variables were kept constant at the nominal operating conditions.

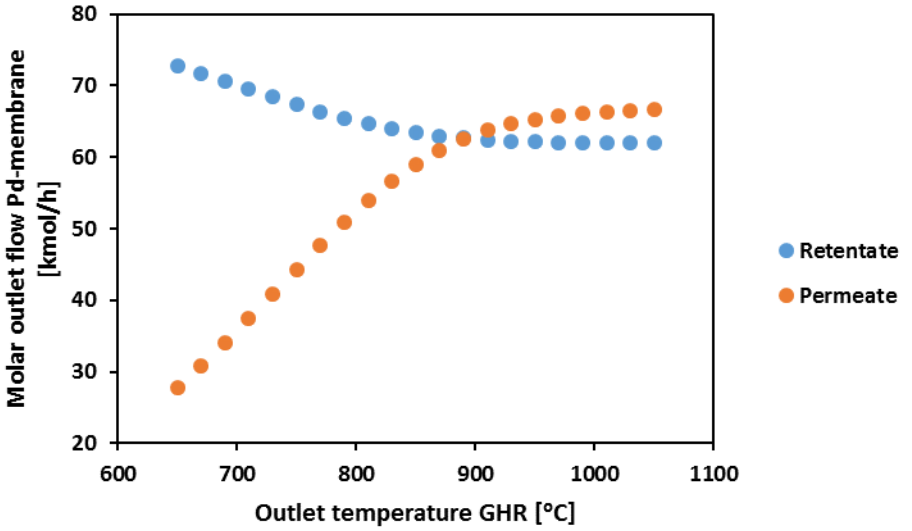

Figure 4.16: Molar outlet flow of the Pd-membrane in the CHP process plotted against the outlet temperature of the GHR. The rest of the variables were kept constant at the nominal operating conditions.

have a rapidly increase before it flattens out, the heat production of the oxyfuel-combustor decreases before it flattens out, but the heat production of the SOFC on the other hand, shows a small decrease before it starts to slightly increase and then flattens out (Fig. 4.14).

The unexpected behaviour of the SOFC may be explained by its internal reformer. As the outlet temperature of the GHR increases, the methane concentration of the SOFC feed decreases. Hence, the internal reformer of the SOFC becomes less energy demanding resulting in the behaviour shown in Fig. 4.14. The reason why this behaviour has not been detected for decreasing operating pressures or increasing S/C ratios may be because it happens around an outlet temperature of 800 °C. At 800 °C the methane conversion of the process is approximately 74%, which is higher than what was achieved for a decreasing operating pressure or an increasing S/C ratio, see Fig. 4.3 and 4.9, respectively.

Fig. 4.17 shows that the electrical power production behave more as expected as the outlet temperature of the GHR increases. As the outlet temperature increases, more hydrogen is passed to the HT-PEMFC while less is passed to the SOFC. Hence, the power production of the HT-PEMFC increases, while the power production of the SOFC decreases. Since the HT-PEMFC has the highest electrical

efficiency of the two fuel cells, the total and net electrical production increase with an increasing outlet temperature of the GHR.

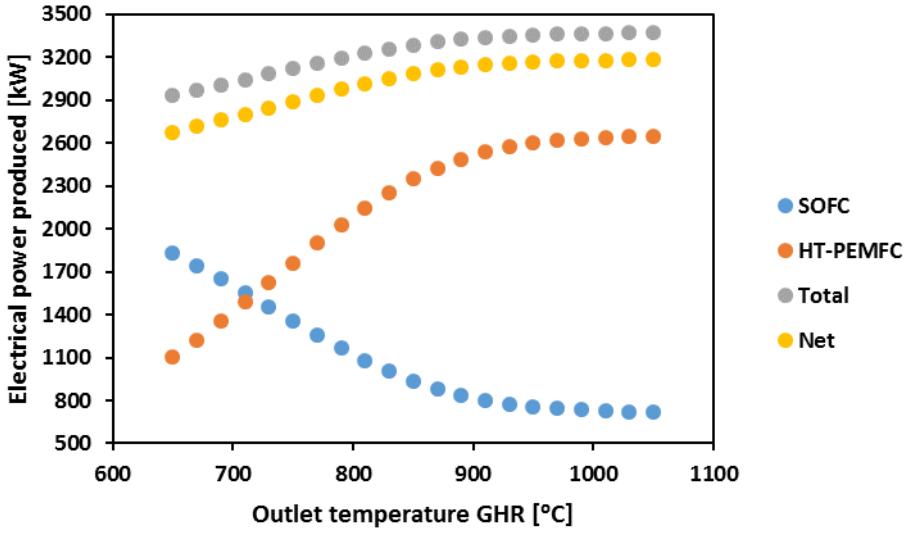

Figure 4.17: Electrical power produced by the two fuel cells in the CHP process plotted against the outlet temperature of the GHR. The rest of the variables were kept constant at the nominal operating conditions.

The above results show that the trade-off between heat and electrical power generation can be shifted towards a better electrical efficiency by increasing the outlet temperature of the GHR. Furthermore, smaller membrane areas are needed as the hydrogen concentration of the reformate increases with an increasing outlet temperature, which is favourable due to costs. However, to increase the outlet temperature of the GHR drastically reduce the production of high quality heat in the process while the energy demand of the reformer is significantly increased.

4.5.4 Hydrogen Recovery

Distribution of load between the two fuel cells in the hybrid fuel cell system has a significant impact on the electrical power generation of the CHP process as the HT-PEMFC have a significantly higher electrical efficiency than the SOFC. In the simulated process, the hydrogen recovery of the Pd-membrane directly controls the fuel supply of the two fuel cells. It was therefore of interest to study how changes in the hydrogen recovery affect the CHP process.

The hydrogen recovery was varied between 50.0% and 90.0%, passing through the nominal condition at 80.0%. Fig. 4.18 shows that the area of the Pd-membrane in-

crease with an increasing hydrogen recovery. As the hydrogen recovery increases, the concentration of hydrogen at the feed side of the membrane decreases, which leads to a lower partial pressure difference of hydrogen across the membrane. As the partial pressure difference decreases, the separation becomes harder and thus the membrane area increases. Furthermore, Fig. 4.18 also shows that above hydrogen recoveries of 80.0%, the membrane area has a more rapidly growth, a result of smaller and smaller partial pressure differences. With the other variables at their respective nominal values, it is not possible to get a better hydrogen recovery than 90.0% as the partial pressure difference becomes too small for further separation.

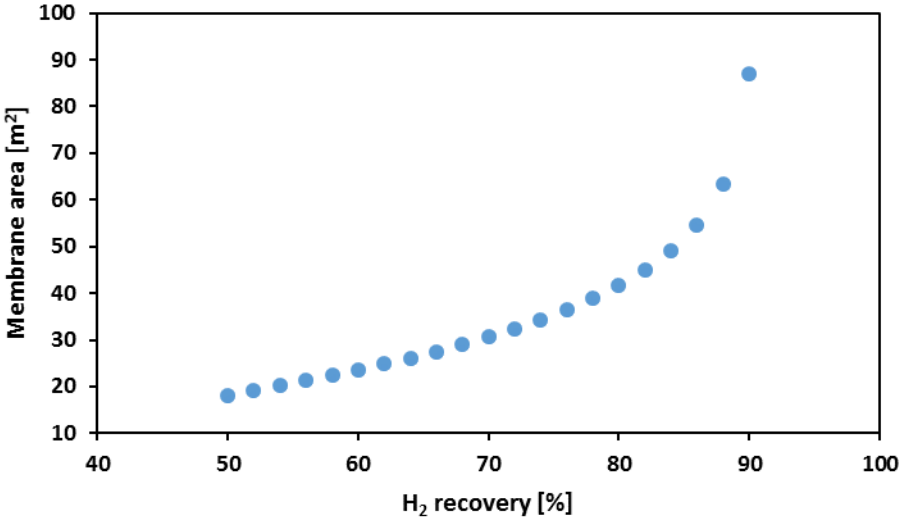

Figure 4.18: Area of the Pd-membrane in the CHP process plotted against the hydrogen recovery. The rest of the variables were kept constant at the nominal operating conditions.

In addition to increase the membrane area, a higher hydrogen recovery also increases the fuel supply of the HT-PEMFC (Fig. 4.19) and thereby the heat and electrical power generation of the HT-PEMFC as well (Fig. 4.20 and 4.21). Since the HT-PEMFC has a higher electrical efficiency than the SOFC, the total and net electrical power production increase with an increasing hydrogen recovery. The trade-off between heat and electrical power generation in the CHP process will therefore be shifted towards a higher electrical power production as the hydrogen recovery increases. However, a bigger hydrogen recovery also results in a bigger membrane area, which means that more exotic material is needed in the membrane.

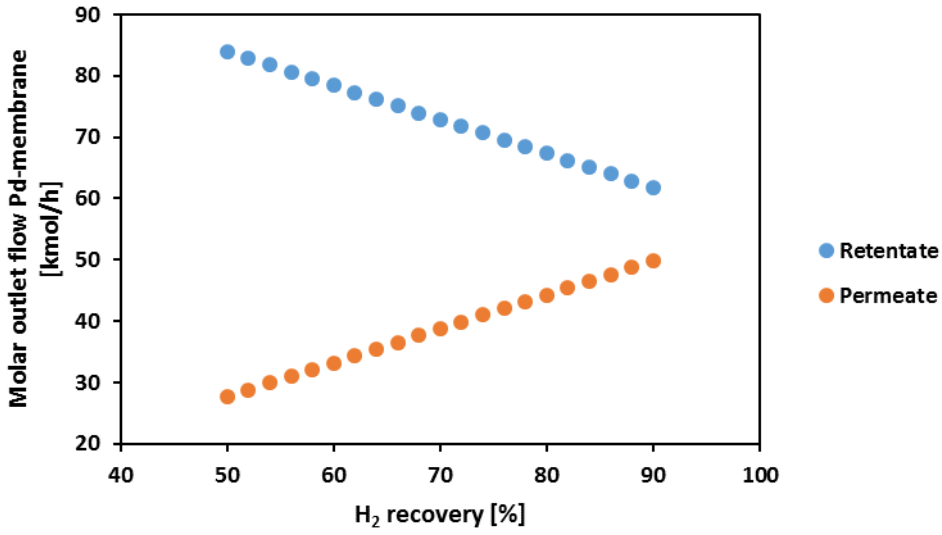

Figure 4.19: Molar outlet flow of the Pd-membrane in the CHP process plotted against the hydrogen recovery. The rest of the variables were kept constant at the nominal operating conditions.

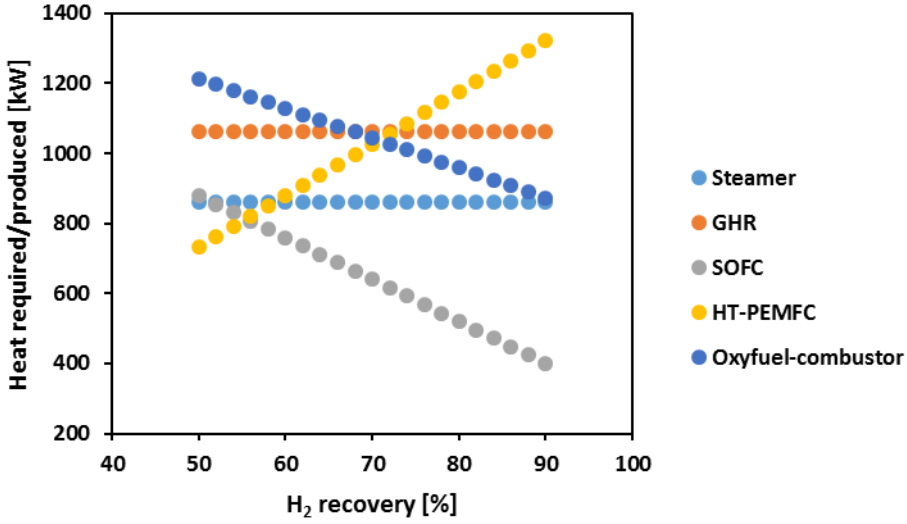

Figure 4.20: Required and produced heat of the different components in the CHP process plotted against the hydrogen recovery. The rest of the variables were kept constant at the nominal operating conditions.

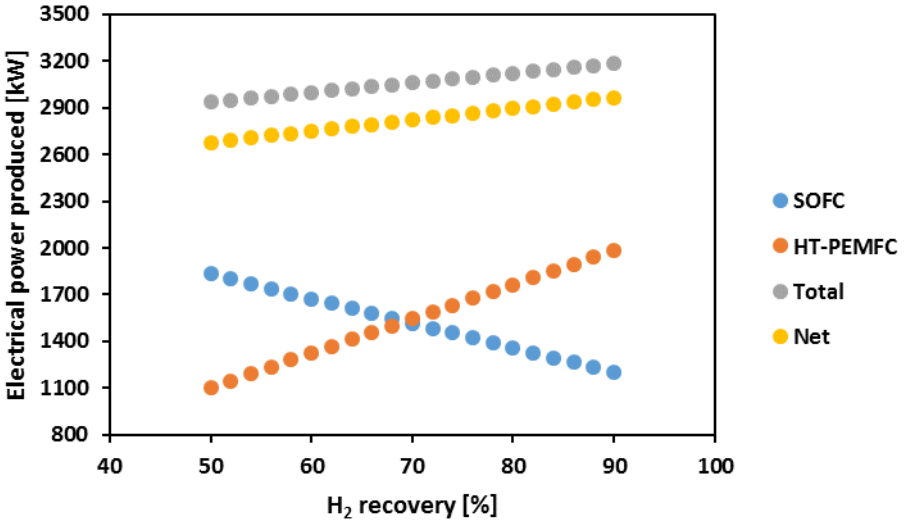

Figure 4.21: Electrical power produced by the two fuel cells in the CHP process plotted against the hydrogen recovery. The rest of the variables were kept constant at the nominal operating conditions.

4.5.5 Conclusion

The sensitivity analysis shows that the trade-off between heat and power production in the CHP process can be shifted towards a higher power production either by decreasing the natural gas feed pressure or by increasing the S/C ratio, the operating temperature of the GHR or the hydrogen recovery of the Pd-membrane as these changes result in a larger fuel supply to the HT-PEMFC. Among these variables, the nominal operating conditions of the natural gas feed pressure, the S/C ratio and the hydrogen recovery are already quite favourable and further improvements might entail other disadvantages: lower feed pressures will increase the size, hence, the cost of the equipment upstream of the hybrid fuel cell system, higher S/C ratios will increase the heat requirements and the size, hence, the cost of the equipment throughout the process as more fluid becomes present while higher hydrogen recoveries will require more exotic material in the membrane as a consequence of higher membrane areas. Hence, the biggest potential to improve the power production and thereby the electrical efficiency of the CHP process, lies in exploiting the excess heat of the system to increase the operating temperature of the GHR.

Chapter 5

Heat Integration

The results of the sensitivity analysis show that there is a potential for further improvements of the electrical efficiency of the GHR process by exploit the excess heat of the process to increase the operating temperature of the GHR. However, these results do not say anything about the amount of excess heat available for heat recovery. Thus, a more rigorously heat integration was performed on the GHR process.

Pinch analysis methods like composite curves (temperature-enthalpy diagram for multi-stream processes), the "Problem Table" method, heat cascades and grand composite curves are all well established heat integration methods for achieving near-optimized process facilities (30, 31, 32). By specifying a minimum approach temperature (ΔT_{min}) of the heat exchangers, the utility requirements, the maximum possible heat recovery, the minimum heat exchanger area and the minimum number of heat exchangers in the process can be established. Based on this, heat exchanger networks (HENs) for maximum energy recovery can be designed and further optimized against cost. Chaves et al. also show how Aspen Energy Analyzer can utilize data from Aspen HYSYS to design HENs and optimize the heat integration (33). However, these methods do not easily integrate heat of chemical reactions and may therefore be considered to be suboptimal for processes that include chemical reactors (34).

Glavič et al. and Karavanja and Glavič have done some work on heat integration of reactors with focus on reactor placement into process flow sheet and total flow sheet integration, but their work ends up in comprehensive optimizations and second-law analysis which is beyond the scope of this thesis (35, 36). The work of Lavric et al. on the other hand, focus on the benefits and drawbacks of chemical

reactors energy integration (CREI) through virtual heat exchangers (VHE) (34). The method is an expansion of the classical pinch analysis which allows to integrate the chemical reactor network (CRN) into the HEN. Their results show that by both including the energy sinks and sources of the CRN into the HEN topology, the CREI analysis gives a methodology towards the lowest entropy producing process in combination with a pinch analysis. However, the analysis do not handle networks with more than two reactors very well.

The CHP process studied in this work includes four reactors: the GHR, the SOFC, the HT-PEMFC and the oxyfuel-combustor. Due to the drawbacks of the methods mentioned above, a more manual approach based on CMR Prototech's design (Fig. 3.1) and the results from Table 4.4 and 4.5 has been used to integrate the reactors, develop a proposed HEN and find the amount of excess heat in the process.

To find the amount of excess heat in the CHP process, two pressurized HEN loops were designed: one high quality heat loop (HQHL, (Fig. 5.1)) where a fluid circulates between the GHR, the SOFC and the oxyfuel-combustor and one low quality heat loop (LQHL, (Fig. 5.3)) where a fluid circulates between the steamer, the HT-PEMFC and other cold streams/components of the process.

Both heat loops were pressurized as it may enable phase change in the respective equipment of the two loops (condensation in the steamer and the GHR and evaporation in the HT-PEMFC and the SOFC) and thereby significantly enhance the heat transfer and reduce the amount of fluid needed in the heat loops. In addition, pressurized heat loops will also contribute to reduce the volume of the gaseous parts of the loops, which together with a phase change will reduce the needed size of the involved equipment and thereby the cost of the process.

On the other hand, pressurized heat loops will also require tube based heat transfer throughout the loops, also in the fuel cells. In addition, one of the main advantages of a HT-PEMFC compared to a LT-PEMFC is water management as water is normally only present as vapour in a HT-PEMFC (37). To pressurize the heat loop such that water enters the HT-PEMFC as liquid may therefore cause flooding problems and affect its performance. If this is the case, the LQHL design has to be changed, nevertheless, since the main purpose of this heat integration was merely to find the amount of excess heat in the CHP process, the LQHL design was kept pressurized as first assumed. Furthermore, both heat loops were designed with pure water and assumed to have no pressure drop, no energy accumulation (steady state) and no heat loss to the surroundings. How the HEN of the two heat loops were developed to find the amount of excess heat in the process are described below.

5.1 High Quality Heat Loop

In the CHP process the reformer is intended to be a gas-heated reformer where heat is supplied by a counter-current heat exchange with a hot gas (water vapour). The hot gas is heated by the SOFC and the oxyfuel-combustor before it is circulated back to the GHR, see Fig. 5.1. Hence, the first step of finding the amount of high quality excess heat in the process, was to find the amount of circulating hot gas needed in the heat loop to supply the energy demand of the GHR.

The inlet and outlet temperature of the GHR, which is represented by stream 5 and 6 in Fig. 5.1, respectively, are given in Table 4.4 and Fig. 5.2. To ensure a sufficient driving force across the reformer, the inlet and outlet temperature of the hot gas, HL3 and HL1 in Fig. 5.1, were set to 950 °C and 550 °C, respectively, see point A in Fig. 5.2. With an assumed hot gas pressure of 20 bar, 227 kmol/h of recirculating water vapour/hot gas was needed to deliver the required amount of heat to the GHR. It is however worth to mention that, since pure water vapour was utilized as hot gas, it was not possible to operate at a pressure that achieved a phase change in the GHR and the SOFC due to the high temperatures of the heat loop. To reduce the amount of fluid needed in the HQHL and thereby the size and cost of the process, it might therefore be of interest to utilize other fluids with the ability to achieve a phase change through the loop.

After the hot gas has been cooled by the GHR it is passed to the SOFC, point B in Fig. 5.1 and 5.2. The SOFC has an operating temperature of 850 °C which delivers 520 kW of heat that brings the temperature of the heat loop up to 750 °C. To raise the temperature of the heat loop the last 200 degrees, the heat loop needs 542 kW of heat from the oxyfuel-combustor (point C in Fig. 5.1 and 5.2), leaving the oxyfuel-combustor exhaust at 936 °C (stream 25.2 in Fig 5.1). However, this is not the correct exhaust temperature of the oxyfuel-combustor as the Gibbs reactor that simulates the oxyfuel-combustor does not convert all the fuel (H_2, CO, O_2) into products (H_2O, CO_2) due to the high temperature of the oxyfuel-combustor exhaust (1400 °C, stream 25.1 in Fig. 5.1). In a real plant however, the conversion would be completed as the temperature of the exhaust decreases in the heat exchanger (C-4), but this is not happening in the simulations. An additional Gibbs reactor was therefore placed after point C to complete the conversion. It resulted in a slightly temperature increase of the oxyfuel-combustor exhaust to 942 °C (stream 25.3 and point F in Fig. 5.1 and 5.2). In point F the oxyfuel-combustor exhaust was cooled down to 550 °C, the outlet temperature of the heat loop in point A (Fig. 5.2) and the oxyfuel-combustor at the nominal operating conditions (Table 4.1 and 4.5), which means that there is 416 kW of high quality excess heat available in the GHR process at the nominal operating conditions.

It is desirable to utilize the excess heat in a way that increase the outlet/operating temperature of the GHR, thus increase the methane conversion of the GHR and thereby the electrical power production of the process. This can be achieved either by having a higher inlet temperature of the recirculating water (hot gas) in the GHR, which can be achieved by heat integrate some of the excess heat with HL1 between the GHR and the SOFC in addition to set a higher outlet temperature of H-6 in point C, or by having more water circulating the loop. The best solution will be a consideration between size and cost requirements.

In addition to increase the hydrogen conversion of the GHR it seems that some of the high quality excess heat might be needed in point D. In point D some of the heat from cooling the WGS feed is utilized to heat the SOFC feed. Even tough the WGS feed have more than enough heat to cover the needs of the SOFC feed (Table 4.4 and 4.5), the heat exchanger approach a pinch in one end as the outlet temperature of SOFC feed approach the inlet temperature of the WGS feed (Fig. 5.2). To ensure a tolerable size and cost of this heat exchanger, some of the excess heat can be utilized in point D.

It is also worth to mention the heat exchange of point E. In point E the heat of the depleted air from the oxygen-pump is utilized to preheat the air feed of the SOFC. From Fig. 5.2 it can be seen that there might be a potential of a higher outlet temperature of the SOFC air feed (H-5), which again will lead to more heat produced in the SOFC and thereby more heat to the heat loop. Even tough the potential might be small, as size and cost of the heat exchanger also need to be considered, this has to be considered in an optimal design.

The HQHL was designed with pure water at 20 bar and temperatures of 550-950 °C. It is worth to mention that it is favourable to design the HQHL with mixtures and pressures that make condensation and evaporation possible in the GHR and the SOFC, respectively, which is not possible with pure water at the given temperatures. Phase change in the GHR and the SOFC will ensure a better heat transfer and significantly reduce the amount of fluid needed in the heat loop. Higher pressures are also favourable as it reduces the size of the gaseous parts of the heat loop.

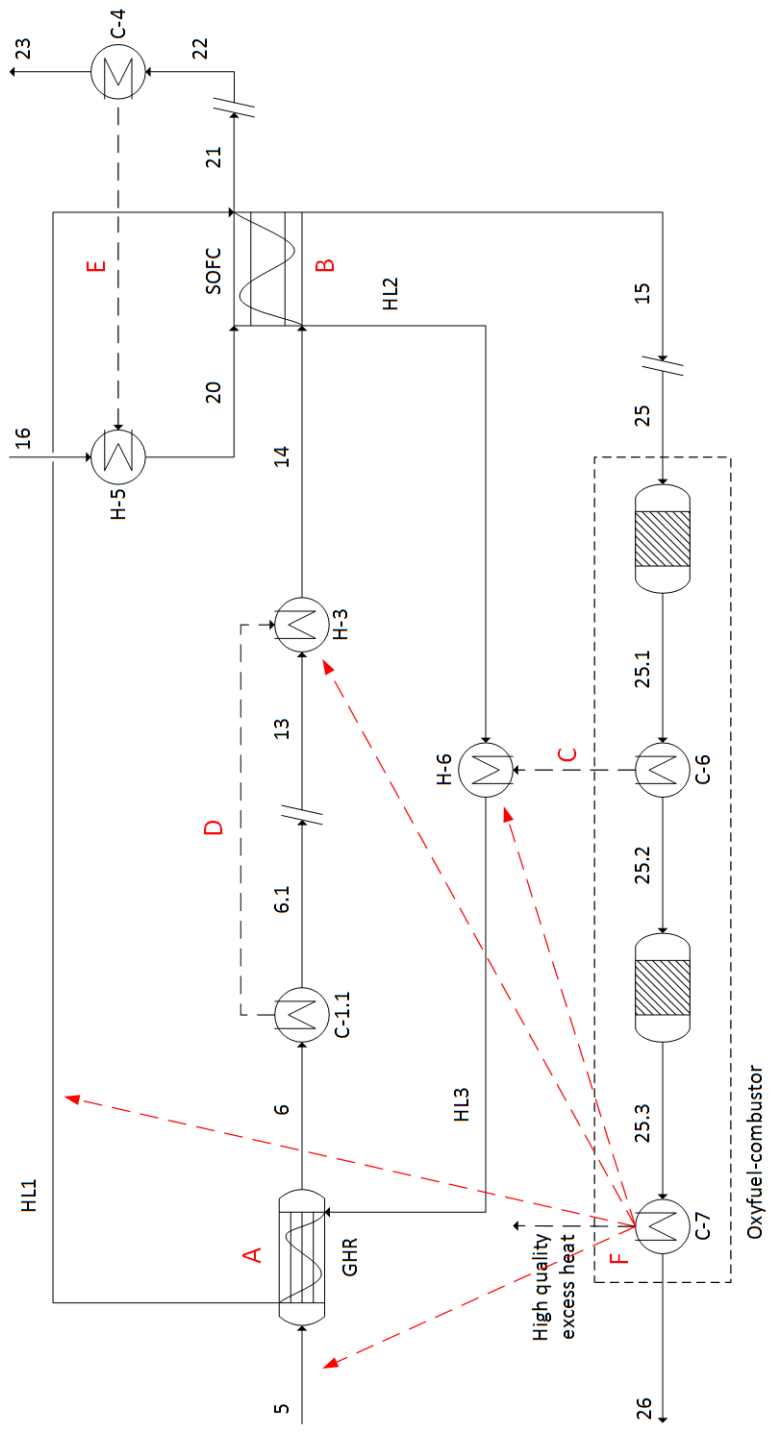

Figure 5.1: Process flow diagram of a suggested high quality heat integration loop between the GHR, the SOFC, the oxyfuel-combustor and the rest of the high quality heaters and coolers of the process. The nomenclature of the figure corresponds to that of Fig. 3.2 and 5.2. The red arrows suggest where the high quality excess heat can be utilized.

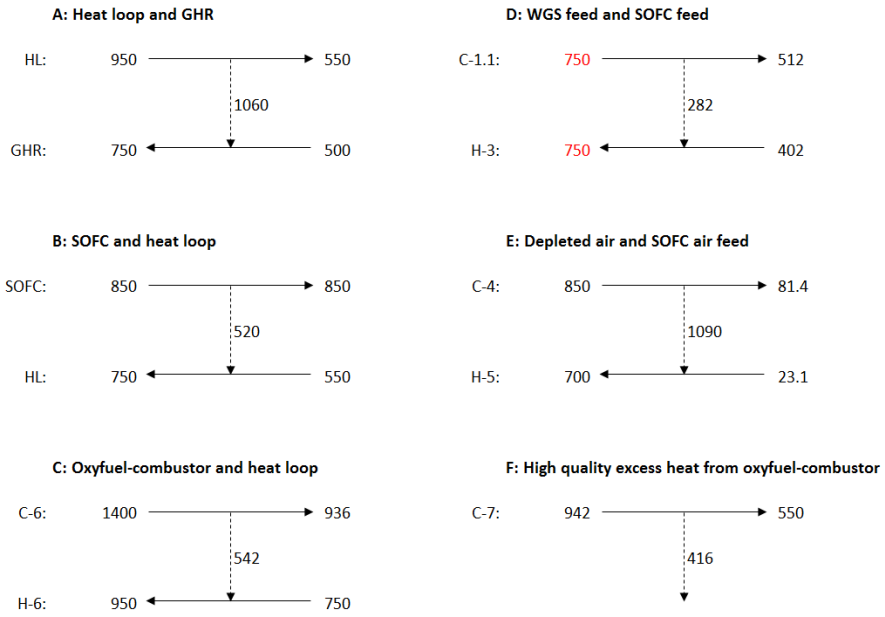

Figure 5.2: Proposed heat integration of the high quality heat loop in Fig. 5.1. The continuous lines represents the material streams of every heat exchange with the respective temperatures given in °C, while the dashed lines represents the heat flows given in kW.

5.2 Low Quality Heat Loop

As for the HQHL, the first step in the heat integration of the LQHL was to find the amount of water recirculating the loop. This was done in the HT-PEMFC, point G in Fig. 5.3 and 5.4. To minimize the amount of water needed in the LQHL, the HT-PEMFC was fed with liquid water pressurized to 5 bar resulting in an inlet temperature of 152 °C. The outlet temperature of the heat loop was sat to 185 °C to ensure a complete evaporation of the water in the loop while still having a sufficient driving force between the HT-PEMFC and the heat loop. With the specified pressure and temperatures, 107 kmol/h of water was needed to utilize the amount of heat available for heat recovery in the HT-PEMFC.

After the HT-PEMFC, the water vapour in the heat loop was heated up to 524 °C by heat exchange with the HT-PEMFC feed, the rest of the heat available in the WGS feed and some of the heat available in the condenser feed, which is represented by point H-I in Fig. 5.3 and 5.4, respectively. With a temperature of 524 °C, the heat loop had enough heat to supply the GHR feed, the pre-reformer feed and the steamer, point K-M in Fig. 5.3, 5.4 and 5.5, respectively, however, it

is worth to notice the small temperature difference between the hot and the cold stream in point L. Furthermore, Fig. 5.5 also shows that a pinch occurs in point P between the HT-PEMFC exhaust and its air feed as the air feed temperature of the HT-PEMFC was set to be equal to the operating temperature of the HT-PEMFC.

After the steamer, there was still some vapour left in the heat loop, hence there is still some unused heat left in the heat loop, see point N in Fig. 5.5. Furthermore, there is also some unused heat left in the condenser feed (point O in Fig. 5.5). As for the high quality excess heat, it is desirable to utilize this low quality excess heat in a way such that the electrical efficiency and/or the cost of the process can be improved. If it is not properly utilized in the process itself or in other low quality heating purposes on the offshore facility, it will contribute to increase the cooling demand of the process.

Due to the temperature the condenser feed possesses, some of its excess heat should be utilized to avoid the pinches in point L and point P of Fig. 5.4 and 5.5, respectively, hence reduce the sizes of these two heat exchangers. After the pinches have been taken care of, some of the remaining excess heat can be utilized to increase the S/C ratio of the GHR process, but this might not be as favourable as first assumed.

The sensitivity analysis of the GHR process shows that if the hydrogen recovery of the membrane is kept constant, higher S/C ratios will increase the energy production of the HT-PEMFC. A higher power production is desirable, but more heat on the other hand will increase the amount of fluid needed in the LQHL and thus increase the size and cost of the equipment connected to the heat loop. As mentioned in the sensitivity analysis, higher S/C ratios will also increase the size and thereby the cost of the equipment throughout the process as more water becomes present in the process. Finally, increased S/C ratios will also increase the energy demand of the GHR, thus utilize some of the high quality heat that could have been used to increase the operating/outlet temperature of the GHR instead. Hence, to utilize the low quality excess heat of the process to increase the S/C ratio in it, might not be the most favourable way to minimize the cooling demand of the process, particularly when size and cost are considered.

Another option that might be more favourable for both the electrical production and the cost of the process, is to increase the electrical efficiency of the HT-PEMFC. An increased electrical efficiency would reduce the amount of heat produced in the HT-PEMFC, hence, reduce the amount of heat available for heat recovery in the HT-PEMFC. This would further reduce the amount of fluid needed, and thereby the size of the equipment in the heat loop, but it would also require that the condenser feed contributes more to supply the low quality heat sinks of the

process, which is not a problem as it turns out.

In the condenser, the condenser feed, which mainly consists of water vapour, is cooled from 200 to 30 °C and thereby actually able to deliver enough heat at sufficient temperatures to supply the steamer by itself. The process does therefore virtually not depend on the heat from the HT-PEMFC to be self-supplied with heat. Hence, the potential for increasing the electrical efficiency of the HT-PEMFC is quite big, at least at the nominal operating conditions of the GHR process. However, an increased efficiency requires a better current and/or a higher operating cell voltage, which again requires a higher hydrogen transport/ionic conductivity and lower polarization losses in the cell. To achieve such conditions in the HT-PEMFC novel materials and designs need to be developed.

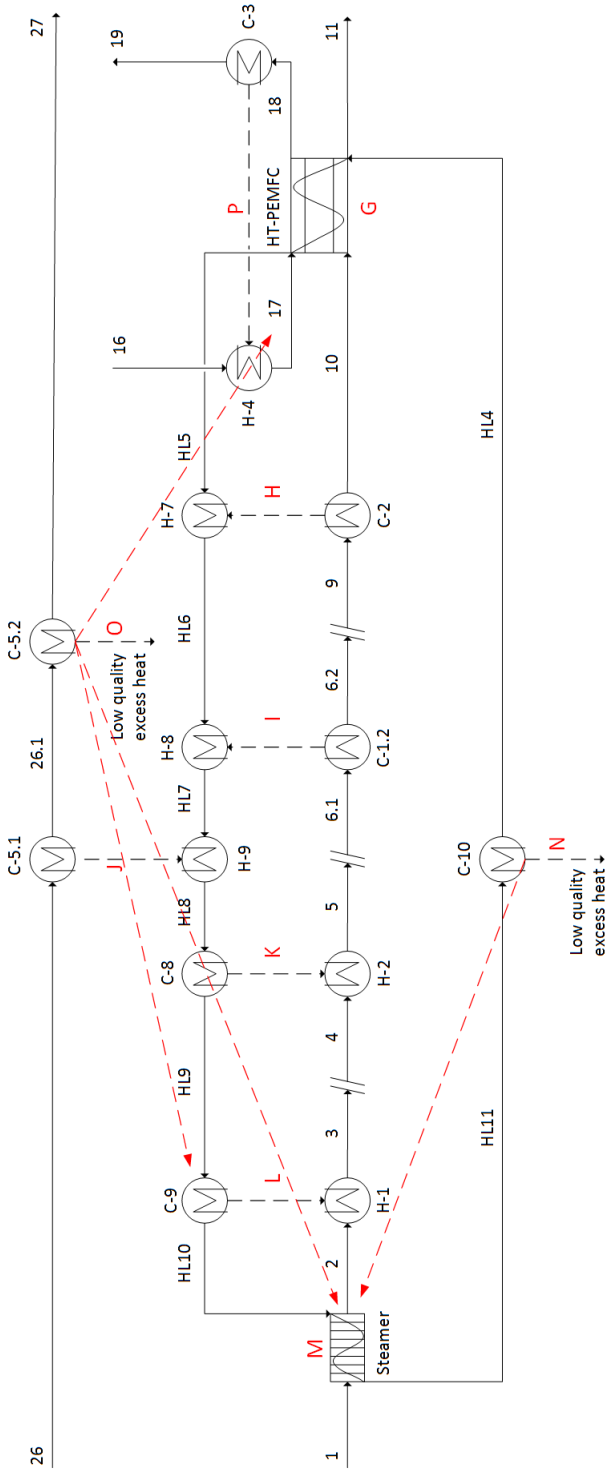

Figure 5.3: Process flow diagram of a suggested low quality heat integration loop between the steamer, the HT-PEMFC and the rest of the low quality heaters and coolers of the process. The nomenclature of the figure corresponds to that of Fig. 3.2, 5.4 and 5.5. The red arrows suggest where the low quality excess heat can be utilized.

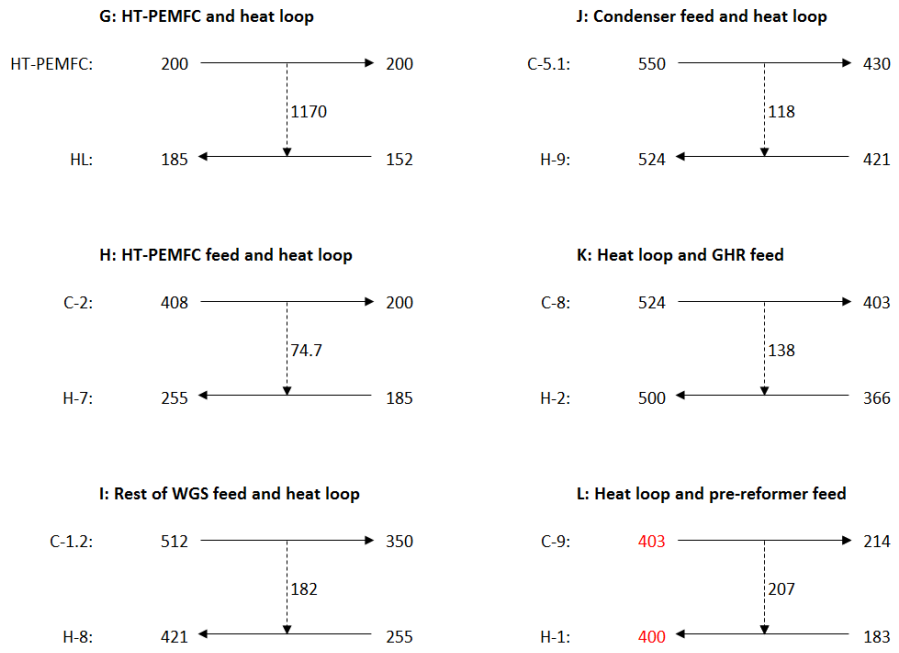

Figure 5.4: Proposed heat integration of the first part (G-L) of the low quality heat loop in Fig. 5.3. The continuous lines represents the material streams of every heat exchange with the respective temperatures given in °C, while the dashed lines represents the heat flows given in kW.

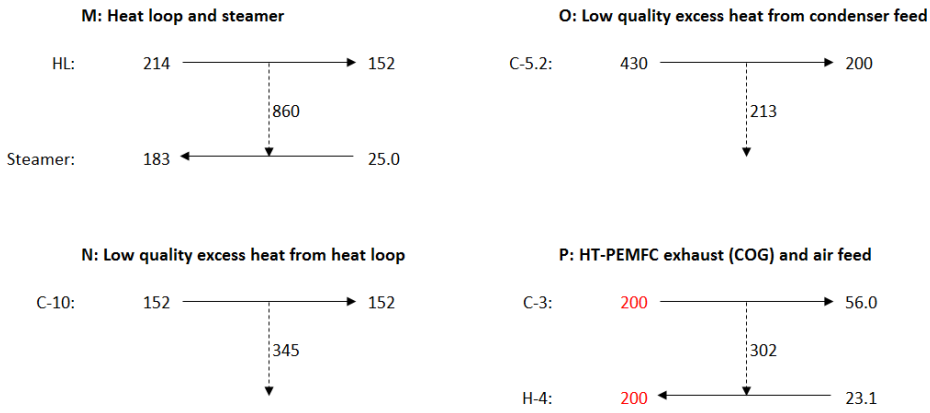

Figure 5.5: Proposed heat integration of the rest (M-P) of the low quality heat loop in Fig. 5.3. The continuous lines represents the material streams of every heat exchange with the respective temperatures given in °C, while the dashed lines represents the heat flows given in kW.

The heat integration of the GHR process shows that there are both high and low quality excess heat available in the process, which means that there is a potential for further improvement of the electrical efficiency of the process. The high quality excess heat can be utilized to increase the operating temperature of the GHR, hence increase the hydrogen production and thereby the power production of the process, while the low quality excess heat can be utilized to increase the S/C ratio, which also will result in a higher hydrogen and power production of the process. Nevertheless, it is important to remember that the values of excess heat mentioned above only apply at the nominal operating conditions and changes in the S/C ratio and the GHR operating temperature highly affect the conditions and performance of the downstream equipment (Pd-membrane, SOFC, HT-PEMFC and oxyfuel-combustor).

Chapter 6

Conclusion and Further Recommendations

In this work, CMR Prototech's proposed hybrid fuel cell process for clean and highly efficient offshore power generation was simulated in Aspen HYSYS to investigate its potential performance with carbon capture. Based on CMR Prototech's P&ID of a scaled-down process, which generates 3.2 MW of electrical power at an efficiency of 60% where the SOFC and the HT-PEMFC module is respectively responsible for 0.7 and 2.5 MW of the total power production, and a more conventional process route for syngas production and hydrogen separation than the membrane reactor used in CMR Prototech's suggested process, an equilibrium based flow-sheet model was developed and implemented in Aspen HYSYS to evaluated the process in this work.

The simulation results show that at the nominal operating conditions, the simulated process gets a net electrical power output of 2.89 MW at an electrical plant efficiency of 56.4%, which is excellent considered that carbon capture is included. However, the SOFC is responsible for approximately 44% of the total power production, which is much more than desired.

A large SOFC is not desirable as size and weight are limiting factors on offshore installations. Since the quick heat integration performed on the process at the nominal operating conditions shows that there is enough heat at sufficient temperatures to supply the process, a sensitivity analysis was performed to study the possibilities of reducing the load and thus the size of the SOFC, which simultaneously implies that the load of the HT-PEMFC will increase and thus also the electrical plant efficiency of the process as the HT-PEMFC has the highest efficiency of the

two fuel cells.

The sensitivity analysis shows that increasing the S/C ratio, the outlet temperature of the reformer and the hydrogen recovery of the Pd-membrane or decreasing the NG feed pressure of the process can contribute to reduce the size of the SOFC as they increase the fuel supply of the HT-PEMFC. However, as the nominal value of the S/C ratio, the NG feed pressure and the hydrogen recovery are already quite favourable and further improvements may imply other disadvantages for the process, the biggest potential to improve the process lies in increasing the outlet temperature of the reformer. A heat exchanger network of both a high and low quality heating was therefore developed to figure out how much excess heat there is in the process.

The heat integrations show that there is approximately 400 kW of high quality excess heat available for utilization in the reformer. If properly utilized this will increase the methane conversion and the hydrogen production of the process, hence, reduce the SOFC load and increase the electrical efficiency of the process. However, even though the 400 kW is utilized, the SOFC is still responsible for a considerable amount of the electrical power generation.

When it comes to the low quality heat loop, there is a lot of excess heat left in the system. Some of this heat can be utilized to increase the S/C ratio of the WGS or to supply the additional heating the product stream of a LT-WGS would require. Both measures would increase the hydrogen production and thereby reduce the size of the SOFC. Since not all of the low quality excess heat can be utilized directly in the process, some of it should be utilized for other low quality heating purposes on the offshore facility. Otherwise it would just contribute to the cooling requirements of the process.

Even though there is both high and low quality excess heat that can contribute to reduce the size of the SOFC in the simulated process, the conventional reforming process chosen in this work is the limiting factor for further reduction of the size of the SOFC. Due to the endothermic nature of the steam reforming process a certain amount of high quality heat is required in the reformer to achieve a certain conversion, hence, a certain load is needed in the SOFC to supply the reformer's energy demand. To reduce the size of the SOFC a less energy demanding reforming unit is needed upstream of the hybrid fuel cell system. Placing membrane reactors upstream of the hybrid fuel cell system, as CMR Prototech initially intended, might therefore contribute to achieve a more desirable performance. It is therefore of huge interest to develop a proper membrane reactor model that can be included in the already existing flow-sheet model to evaluate if the desired distribution of load can be achieved in further work.

Another interesting observation that was made during the heat integration was the potential for further improvements in the efficiency of the HT-PEMFC. Due to the amounts of excess heat available in the condenser feed, the process can function just fine without most of the heat produced in the HT-PEMFC. If the electrical efficiency of the HT-PEMFC is increased, some of this excess heat will instead be utilized to produce electrical power. This will not contribute to reduce the size of the SOFC, but it will contribute to reduce the size of the HT-PEMFC and hence the total weight of the hybrid concept in addition to increase the overall efficiency of the process and thus reduce the amount of fuel needed in the process. However, to increase the efficiency of the HT-PEMFC will require novel technology in terms of unit cell materials and stack design, but recommended to investigate in further work due to the potential for further improvements.

Bør kanskje også si noe om at simuleringene er basert på likevekt og kan defor være litt optimistiske (hvis vi ikke oppnår likevekt). Videre arbeid bør det vurderes å bassere simuleringene på kinetikk og varmeoverføringsmodeller i reaktorer og i cellene. I cellene bør man kanskje også ta hensyn til trykktap og basere simuleringene på elektrokjemiske modeller slik at de kan sizes. Size og cost bør gjøres i videre arbeid.

Bibliography

[1] C. W. Team, R. Pachauri, and L. M. (eds.), *IPCC, 2014: Climate Change 2014: Synthesis Report. Contribution of Working Groups I, II and III to the Fifth Assessment Report of the Intergovernmental Panel on Climate Change*. IPCC, Geneva, Switzerland, 151 pp., 2014.

[2] Miljødirektorate, "Norske utslipp av klimagasser." http://www.miljostatus.no/tema/klima/norske-klimagassutslipp/. Accessed: 09.11.2016.

[3] K. A. Rosvold and A. Vinjar, "Gasskraftverk." https://snl.no/gasskraftverk. Accessed: 06.04.2017.

[4] S. Lundberg and K. E. Kaski, "Strøm fra land til olje- og gassplattformer," tech. rep., ZERO, 2011.

[5] K. Hofstad, "Kombikraftverk." https://snl.no/kombikraftverk. Accessed: 06.04.2017.

[6] Miljødirektorate, "Klimagassutslipp fra olje og gass." http://www.miljostatus.no/tema/klima/norske-klimagassutslipp/klimagassutslipp-olje/. Accessed: 09.11.2016.

[7] E. Martiniussen and J. Løvås, "Kraftkampen." http://www.dn.no/magasinet/2014/05/09/Elektrifisering-av-sokkelen/kraftkampen. Accessed: 06.04.2017.

[8] P. Qvale, "Elektrifisering offshore har ingenting for seg." https://www.tu.no/artikler/elektrifisering-offshore-har-ingenting-for-seg/225240. Accessed: 06.04.2017.

[9] "Kraft fra land til norsk sokkel," tech. rep., NVE, OD, SFT, Ptil, 2008.

[10] A. Torvanger and T. B. Ericson, "Fører elektrifisering av plattformer på norsk sokkel til reduserte CO_2-utslipp?," tech. rep., CICERO, 2013.

[11] Øyvind Lie, "Øker kostnaden på elektrifisering fra 6,5 til 13,2 milliarder." https://www.tu.no/artikler/oker-kostnaden-pa-elektrifisering-fra-6-5-til-13-2-milliarder/231401. Accessed: 06.04.2017.

[12] "Clean highly efficient offshore power (cheop)." http://cmr.no/projects/10454/clean-highly-efficient-offshore-power-cheop/. Accessed: 06.04.2017.

[13] "Samarbeider om energismarte løsninger for offshore-utbygginger." http://offshore.no/sak/246419_samarbeider-om-energismarte-losninger-for-offshore-utbygginger. Accessed: 06.04.2017.

[14] M. Valle, "Norskutviklet løsning skal sørge for CO_2-fri strøm offshore - uten å legge strømkabel fra land." https://www.tu.no/artikler/norskutviklet-losning-erstatter-gassturbiner-offshore-med-hydrogen/378713?key=8x2CMhKt. Accessed: 06.04.2017.

[15] K. Liu, C. Song, and V. Subramani, *Hydrogen and Syngas Production and Purification Technologies*. Wiley-AlChE, 2009.

[16] S. D. Angeli, G. Monteleone, A. Giaconia, and A. A. Lemonidou, "State-of-the-art catalysts for CH_4 steam reforming at low temperature," *International Journal of Hydrogen Energy*, vol. 39, pp. 1979–1997, 2014.

[17] M. Voldsund, K. Jordal, and R. Anantharaman, "Hydrogen production with CO_2 capture," *International Journal of Hydrogen Energy*, vol. 41, pp. 4969–4992, 2016.

[18] J. Xu and G. F. Froment, "Methane steam reforming, methanation and water-gas shift: I. Intrinsic kinetics," *AlChE Journal*, vol. 35, pp. 88–96, 1989.

[19] T. M. Gür, "Comprehensive review of methane conversion in solid oxide fuel cells: Prospects for efficient electricity generation from natural gas," *Progress in Energy and Combustion Science*, vol. 54, pp. 1–64, 2016.

[20] S. D. Angeli, F. G. Pilitsis, and A. A. Lemonidou, "Methane steam reforming at low temperature: Effect of light alkanes' presence on coke formation," *Catalysis Today*, vol. 242, pp. 119–128, 2015.

[21] M. A. Nieva, M. M. Villaverde, A. Monzón, T. F. Garetto, and A. J. Marchi, "Stem-methane reforming at low temperature on nickel-based catalysts," *Chemical Engineering Journal*, vol. 235, pp. 158–166, 2014.

[22] P. Moriarty and D. Honnery, *Hydrogen Production: Prospects and Processes*. Energy Science, Engineering and Technology, Nova Science Publishers, Inc, 2012.

[23] N. Al-Mufachi, N. Rees, and R. Steinberger-Wilkens, "Hydrogen selective membranes: A review of palladium-based dense metal membranes," *Renewable ans Sustainable Energy Reviews*, vol. 47, pp. 540–551, 2015.

[24] S. Kluiters, "Status review on membrane systems for hydrogen separation," *Intermediate report EU project MIGREYD NNE5-2001*, 2004.

[25] X. He and M.-B. Hägg, "Membranes for Environmentally Friendly Energy Processes," *Separation Science and Technology*, vol. 2, pp. 706–726, 2012.

[26] Z. Tao, L. Yan, J. Qiao, B. Wang, L. Zhang, and J. Zhang, "A review of advanced proton-conduction materials for hydrogen separation," *Progress in Materials Science*, vol. 74, pp. 1–50, 2015.

[27] F. Barbir, *PEM Fuel Cells, Theory and Practice*. Elsevier, 2013.

[28] O. Z. Sharaf and M. F. Orhan, "An overview of fuel cell technology: Fundamentals and applications," *Renewable and Sustainable Energy Reviews*, vol. 32, pp. 810–853, 2014.

[29] S. Campanari, L. Mastropasqua, M. Gazzani, P. Chiesa, and M. C. Romano, "Predicting the ultimate potential of natural gas SOFC power cycles with CO_2 capture - Part A: Methodology and reference cases," *Journal of Power Sources*, vol. 324, pp. 598–614, 2016.

[30] I. C. Kemp, *Pinch Analysis and Process Integration*. Butterworth-Heinemann, 2007.

[31] R. Sinnot and G. Towler, *Chemical Engineering Design*. Coulson & Richardson's Chemical Engineering, Butterworth-Heinemann, 2009.

[32] J. J. Klemeš, *Handbook of Process Integration*. Woodhead Publishing Series in Energy, Elsevier Science, 2013.

[33] I. D. G. Chaves, J. R. G. López, J. L. G. Zapata, A. L. Robayo, and G. R. Niño, *Process Analysis and Simulation in Chemical Engineering*. Springer, 2016.

[34] V. Lavric, V. Plesu, and J. D. Ruyck, "Chemical reactors energy integration through virtual heat exchanges - benefits and drawbacks," *Applied Thermal Engineering*, vol. 25, pp. 1033–1044, 2005.

[35] P. Glavič, Z. Kravanja, and M. Homsak, "Heat integration of reactors - I. Criteria for the placement of reactors into process flowsheet," *Chemical Engineering Science*, vol. 43, no. 3, pp. 593–608, 1988.

[36] Z. Kravanja and P. Glavič, "Heat integration of reactors - II. Total flowsheet integration," *Chemical Engineering Science*, vol. 44, no. 11, pp. 2667–2682, 1989.

[37] S. Authayanun, K. Im-orb, and A. Arpornwichanop, "A review of the development of high temperature proton exchange membrane fuel cells," *Chinese Journal of Catalysis*, vol. 36, pp. 473–483, 2015.